DEPENDENCE OF STRENGTH ON CORROSION-FATIGUE RESISTANCE OF AISI 4130 STEEL

A Thesis
Presented to
The Academic Faculty

By

Joseph Lee Evins

In Partial Fulfillment
Of the Requirements for the Degree
Master of Science in Mechanical Engineering

Georgia Institute of Technology
April 2004

DEPENDENCE OF STRENGTH ON CORROSION-FATIGUE RESISTANCE OF AISI 4130 STEEL

Prof. Ashok Saxena, Chairman

Prof. Richard W. Neu

Prof. Preet Singh

Prof. W. Steven Johnson

Date Approved: April 9, 2004

ACKNOWLEDGEMENTS

First and foremost, I would like to thank my parents, Lee and Barbara, for all of their support. Without them I certainly would not be where I am today. Through their emotional and financial support I have had many opportunities that I never thought possible. This thesis is dedicated to them and the sacrifices that they made for me.

I would also like to thank my co-advisors for this project, Professor Ashok Saxena and Professor Rick Neu. Professor Saxena selected me for this project and provided the guidance and direction for the research. Professor Neu was very helpful in the final months of the preparation of the thesis. His time and advisement were very much appreciated.

My thesis reading committee also deserves appreciation. In addition to my two co-advisors, Professor Steve Johnson and Professor Preet Singh provided their time and assistance in completing this project. Professor Johnson has been kind to allow me to reside in his Bunger-Henry office for the duration of my project. Professor Singh's advice on the corrosion aspects of my writing was very helpful.

My project sponsor, the Goodyear Tire and Rubber Company in Akron, Ohio, also deserves credit for the success of this project. Dr. Amit Prakash of Goodyear was a great source of guidance and motivation for this work and was kind to allow me to spend a summer directly researching with him in Akron.

The laboratory technician, Rick Brown, provided useful experimental setups and helpful guidance on conducting accurate tests. He also provided help with troubleshooting and all equipment issues that arose during testing.

My fellow graduate students that shared Professor Johnson's Bunger-Henry office also deserve credit. Matt Pavlick has been a good person to know during my research experience. He has been a great source of information about classes and thesis writing, as well as, a good friend. The other graduate students that were in the office came and went, however, the current students, Matt Hammond and Carrell Weeks are a lot of fun and made the work enjoyable.

My girlfriend, Sara King, and all of my friends and family also deserve a lot of credit for dealing with me through the ups and downs that have come with the project. In this case, the phrase, "I couldn't have done it without them" has never been more appropriate.

TABLE OF CONTENTS

LIST OF TABLES

LIST OF FIGURES

LIST OF SYMBOLS AND ABBREVIATIONS

^{o}	degrees
^{o}C	degrees Celsius (Centigrade), unit of temperature
^{o}F	degrees Fahrenheit, unit of temperature
ε	strain
μ	micro, 10^{-6}
ν	Poisson's ratio
σ	stress
σ_{ult}	ultimate tensile stress
σ_{y}	yield stress
$\sigma_{y\ (0.2\%)}$	0.2% offset yield stress
AISI	American Iron and Steel Institute
ASM	American Society for Metals
ASTM	American Society for Testing and Materials
CFC	Corrosion-fatigue Cracking
CFCI	Corrosion-fatigue Crack Initiation
CTL	Cincinnati Testing Labs
DI Water	de-ionized water
E	Young's elastic modulus
EIC	Environment-Induced Cracking
et al.	latin, "and others," when referring to multiple authors
g	grams, metric units of mass

HIC	Hydrogen-Induced Cracking
in.	inch, unit of length
ISO	International Organization for Standardization
kip	1000 pounds-force
ksi	1000 pounds per square inch
lb	pound, unit of either mass or force
m	meter, unit of length
M.E.	Mechanical Engineering
min	minute, unit of time
mm	millimeter, unit of length
MPa	megapascal, units of pressure
MPRL	Mechanical Properties Research Lab, Georgia Tech
MSE	Material Science and Engineering
MTI	company, Measurements Technology, Inc.
MTS	company, Mechanical Testing and Simulation
N	Newton, metric unit of force
P	load
P_{max}	maximum load during a tensile test
psi	pounds per square inch, units of pressure
RT	room temperature, defined for this thesis as 26^{o}C (78^{o}F)
S_a	Stress Amplitude
S_m	Mean Stress
S_r	Stress Range

SAE	Society of Automotive Engineers
SCC	Stress Corrosion Cracking
SEM	Scanning Electron Microscope
SI	International System of Units (metric)
vs.	versus

SUMMARY

Automobile components are often exposed to aggressive environments as a result of aqueous salts from the road coming into contact with unprotected steel. This situation greatly reduces both the life and the appearance of the affected parts. Ultra-high strength steel parts are suspected to exhibit poor corrosion-fatigue properties and be more susceptible to corrosion in general.

In this study, the effect of strength level on the decrease in fatigue life of AISI 4130 steel when exposed to an aqueous salt solution is quantified. The observed mechanical properties including corrosion-fatigue behavior are examined with consideration to different microstructural characteristics resulting from heat treatments to the steel. The hardness and tensile properties of the test material were characterized before fatigue testing. Fatigue tests were completed in both air and salt solution to determine the effect on fatigue life of the latter environment. Following fatigue testing, the fracture surface was examined using a scanning electron microscope (SEM) to determine the failure mode.

Six strength levels of AISI 4130 steel were investigated ranging from 837 to 1846 MPa (121 – 268 ksi). The frequency of loading used for corrosion-fatigue tests was 1 Hz and the stress ratio for each test was constant at R = 0.1. The corrosion-fatigue tests consisted of the specimen being submerged in an aqueous solution of sodium chloride, calcium chloride, and sodium bicarbonate and fatigued until failure. The solution was maintained at room temperature with constant aeration to ensure constant oxygen levels. The parameters of interest were the applied loads and the cycles to failure.

There were four primary findings of the study. First, decreases in fatigue life of the material caused by the corrosive environment ranged from 100% in the lowest strength level to 190% in the higher strength levels. This result showed that higher strength in this steel corresponds to increasing detriment to fatigue life when the material is exposed to an aqueous salt environment. Second, evidence was found that the salt solution lowered the fatigue limit for each strength level studied in this material. All specimens that were tested in the corrosive environment failed in less than 150,000 cycles, while some specimens fatigued in the air environment experienced run-outs at over 10^6 cycles. Third, the decrease in fatigue life was attributed to the presence of martensite in the structure of the steel. It was noted that the higher the martensite content, the larger the decrease in fatigue life when exposed to the corrosive environment. Finally, the fracture surfaces of fatigued specimens revealed that a similar cracking mode was present for each strength level in both environments. Enhanced crack initiation was, therefore, assumed to be the cause of the decrease in fatigue life between the air and aqueous salt environments.

CHAPTER I

INTRODUCTION AND RESEARCH OBJECTIVES

In automobile components where steel is exposed to aqueous salts from the road, the effects of corrosion are often an important design consideration. The problem is compounded by the fact that designers now require higher strength and lower weight from components. Heat treatment is one approach to obtain higher strength without increasing weight. However, as steel is quenched and tempered to increase its strength, its corrosion-fatigue resistance decreases. Therefore, there is an obvious trade-off between high strength and the material's inability to perform well in corrosive environments. Thus, automotive engineers are interested in optimizing the strength of alloy steels while maintaining good corrosion resistance.

An application that would benefit from an optimum level of strength and corrosion resistance is automotive wheels. A current initiative by automotive wheel assembly manufacturers includes using an ultra-high strength steel to build a compliant rim. This rim would be required to support the loads of standard rims but provide deflection to aid in smoothing the ride of the vehicle. In order for the spokes to operate within their elastic region, they must have very high strength. Also, the material is required to be formable and weldable. Medium-carbon low-alloy steel fulfills these requirements, however, at high strength levels, this steel is susceptible to corrosion and hereby reductions in the corrosion-fatigue properties.

The objective of this research is to determine the decrease in fatigue life associated with immersion of AISI 4130 steel in an aqueous sodium chloride based

environment. Mechanical properties and corrosion susceptibility are strongly influenced by heat treatment. The current study investigates heat treatments that result in tensile strengths ranging from 896 MPa to 1862 MPa (121 – 268 ksi). The fatigue lives obtained from tests conducted in the corrosive media are compared to those conducted in laboratory air to quantify the effect of the corrosive media and heat treatment on fatigue life.

The following chapters contain the details of this study. Chapter II provides an overview of the corrosion process and of general trends in the corrosion-fatigue behavior of low-alloy steel. Specific work completed in this area is also outlined and discussed. Chapter III describes the characteristics of the material, the test specimen geometry, and the heat treatment and fabrication of the specimens. In Chapter IV, the experimental test equipment and test procedures for the tensile, hardness, and fatigue tests are examined. Experimental results from these tests are presented in Chapter V. This chapter also includes a discussion of the results where the data is analyzed and general trends are revealed. The conclusions drawn from this work are listed in Chapter VI. Chapter VII outlines recommendations for future work.

CHAPTER II

BACKGROUND AND LITERATURE REVIEW

In an investigation of the effects associated with low-alloy steel in a corrosive environment, one must first understand what work has been done in the past and how the current work fits into the field in general. To establish a framework for the present study, the basic processes involved in corrosion and corrosion-fatigue are reviewed. Then, specific examples are outlined to demonstrate basic trends found in the literature. A thorough review of all information related to corrosion-fatigue could fill many books. Therefore, only an overview of the topic is included in this study.

2.1 Corrosion Effects Associated with Aqueous Salt Environment

To study corrosion-fatigue, a multidisciplinary approach is needed that involves chemistry, mechanics, and metallurgy. In this section, the chemistry and mechanics that cause corrosion related failures are studied. First, the various forms of corrosion that lead to failure in steel are reviewed along with chemistry that causes them. Then, the mechanisms responsible for the effects of corrosion-fatigue are summarized.

2.1.1 Forms of Corrosion that Lead to Failure

In 1966, Marcel Pourbaix demonstrated that a metal could react in one of four ways when exposed to a corrosive fluid.[1] By varying electrode potential and pH of the solution, he was able to create what are called Pourbaix diagrams that demonstrate the corrosion activity that is thermodynamically favored in a given system. An example of a Pourbaix diagram for an iron-water system at 25 °C is shown in Figure 2.1. The diagram

is divided into four areas that represent the ways that a metal can react to a corrosive fluid. He proposed that a metal could be immune from chemical reaction, show active corrosion, display passivity due to formation of a protective oxide film, or suffer from pitting corrosion due to localized breakdown of a passive film. While the basic trend is the same for all Pourbaix diagrams, each is specific to a particular metal-fluid system.

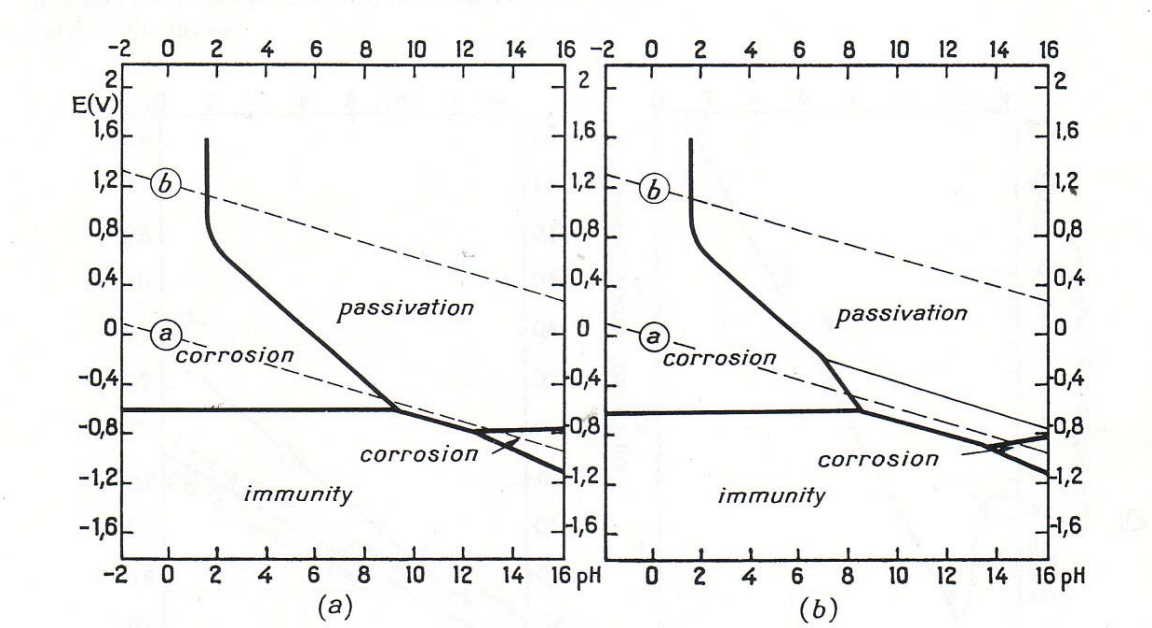

Figure 2.1. Theoretical conditions of corrosion, immunity, and passivation of iron[1]
(a) assumes passivation by a film of Fe_2O_3,
(b) assumes passivation by films of Fe_2O_3 and Fe_3O_4.

If a metal is not immune to a given environment, the governing chemistry dictates that the metal is consumed in an anodic reaction, and electrons are removed by a cathodic reaction. The two cathodic reactions that are most often observed in metals are the reduction of oxygen to hydroxyl ions in aerated solutions or the hydrogen evolution reaction in de-aerated solutions.[2] These chemical reactions result in one of three reaction possibilities according to Pourbaix: active corrosion, passivity, or pitting. With the

exception of stainless steel, most steels do not show passivity and are, therefore, consumed by active corrosion or pitting.

Active corrosion and pitting can lead to failure in steel. However, other corrosion effects have been observed to cause the failure of steel. The term Environment-Induced Cracking (EIC) is used to represent these effects. EIC includes stress corrosion cracking (SCC), hydrogen-induced cracking (HIC), and corrosion-fatigue cracking (CFC).

Stress corrosion cracking (SCC) is observed in metals subjected to a sustained constant tensile stress in the presence of a corrosive fluid. The corrosion rate in SCC is usually quite low since the material that is oxidized on the surface provides a surface film through which the corrosive species must diffuse to further oxidize the material.

Hydrogen-induced cracking (HIC) is a failure mechanism more often observed in low-alloy and stainless steels than the SCC mode. HIC is observed when hydrogen is diffused into the alloy lattice. This causes hydrogen embrittlement in the material surrounding the crack that allows further propagation of the crack. According to Suresh, the mechanism for hydrogen embrittlement in an aqueous environment can be described as six-part process: (1) Water molecules or hydrogen ions diffuse to the crack tip. (2) Electrons are discharged and reduced at the crack tip wall. (3) Hydrogen atoms are adsorbed to the crack surface. (4) The hydrogen adatoms are then diffused to surface locations that are ideal for corrosion activity. (5) The hydrogen absorbs into the metal and (6) diffuses into the material ahead of the crack tip.[3] A diagram is included in Figure 2.2 illustrating this reaction.

Another corrosion effect found to cause failure in steels is corrosion-fatigue cracking (CFC). It is observed when the effects of either SCC or HIC are coupled with

fluctuating loading. This combination results in a synergistic relationship that causes far greater degradation in material load carrying capability than is observed from either effect alone or from a linear superposition of the individual effects.[4]

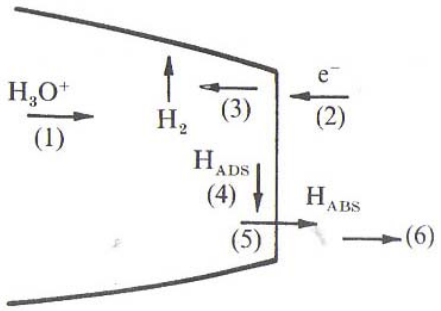

Figure 2.2. Steps involved in hydrogen embrittlement in an aqueous environment [3]

2.1.2 Corrosion-Fatigue Mechanisms

Studies dating back to the work of Gough & Sopwith (1932) and Thompson, Wadsworth, and Louat (1956) show that oxygen containing aqueous media generally reduce the fatigue lives of ductile solids.[3] A study by Scott found that the initiation and propagation phases of fatigue crack growth are likely to be more affected by environment than the final catastrophic failure phase.[2] Therefore, crack initiation mechanisms are very important in the study of corrosion-fatigue life. Four mechanisms have been suggested that cause faster crack initiation when steel is exposed to a corrosive environment. These mechanisms are listed below:

1. Corrosion pits leading to stress concentrations
2. Preferential electrochemical attack at locations on the surface of fatigued metal where plastic deformation is localized
3. Rupture of an oxide film
4. A reduction in the surface energy of the alloy as a consequence of the adsorption of the environmental species

Each of these mechanisms serves to explain some of the aspects of the corrosion-fatigue phenomena; however, none of them completely encompass the solution. The following is a discussion of each proposed mechanism.

The stress concentration resulting from corrosion pits was one of the first mechanisms proposed to explain the faster crack initiation that is observed in corrosion-fatigue. McAdam first proposed the idea in 1928. By investigating failed corrosion-fatigue specimens, McAdam found that fatigue cracks that eventually lead to failure were observed propagating out of corrosion pits. Pit formation has been linked to decreases in fatigue life, but decreases are also seen in materials and environments that do not exhibit pit formation.[5] Duquette and Uhlig investigated low carbon steels in neutral 3% NaCl solution and found that the pitting that was present was not the cause of cracks found in the surface.[5] Laird and Duquette generalized this observation and claimed that the pits observed at failure by previous researchers are not the cause of corrosion-fatigue cracking but rather the result.[5] Therefore, other mechanisms were sought to explain these observations.

The preferential dissolution mechanism is also proposed to cause a decrease in corrosion-fatigue initiation life. In this theory, fresh metal exposed when slip steps break the surface of a specimen is preferentially attacked by the corrosive species. This attack creates stress concentrations in this already highly strained area that cause decreases in the fatigue strength of the material. U. R. Evans has demonstrated that highly deformed areas in metals and alloys, such as areas of slip steps, are anodic to undeformed areas. Even though the reaction proposed by Evans is not thermodynamically favored, the fresh metal is believed to have lower activation energy that allows the metal to react with the

corrosive solution.[5] This mechanism naturally relies on the metal exhibiting slip steps on the surface of the material. Therefore, if the fatigued material not prone to slip steps, the preferential dissolution mechanism may be irrelevant.

The rupture of oxide films can also cause faster crack initiation in certain metals and environments. This effect is primarily found in materials such as copper, aluminum, and stainless steels where an oxide layer is formed as a result of contact with air. Since most steels other than stainless steels do not exhibit this behavior, this mechanism will not be investigated further.

The final mechanism investigated in this review is the reduction of the surface energy of an alloy as a result of adsorption of environmental species. This effect has been termed the Rebinder mechanism. Rebinder and his associates showed that metals coated with a surface-active agent like oleic acid showed accelerated creep rates.[5] The original theory suggested that the surface-active agent adsorbed into microcracks that were present in the material and increased the pressure within the cracks to effectively advance the crack at reduced global stresses. Later, Rebinder modified this theory to state that the adsorbing species reduced the surface energy of the material, thereby making it easier to create protruding slip bands on the metal surface.[5] Another modification was made in 1955 when Karpenko claimed that two distinct steps were involved in corrosion-fatigue crack initiation. The first was a crack initiation process similar to Rebinder's mechanism. The second was a corrosion process occurring within initiated cracks.[5] While this modification eliminates some criticism of Rebinder's theory, there is not much evidence to support it. In general, the reduction in surface energy

mechanism is a plausible theory, but it is not able to explain all phenomena associated with reduced corrosion-fatigue crack initiation life.

Each of the corrosion-fatigue crack initiation mechanisms discussed above have good basis for explaining effects observed in corrosion-fatigue; however, it has been shown that each can not fully explain every case. Corrosion pitting is observed to reduce the corrosion-fatigue life of steel, but the same decrease is observed in absence of pitting. Preferential dissolution is prevalent in materials where slip steps protrude from the material surface, but this mechanism cannot explain the effects in materials that are not prone to this behavior. As discussed above, the rupture of oxide films is not applicable to most steels where these films are not observed. Finally, the Rebinder mechanism is the most plausible of the four, but it cannot explain all effects. In steels that show a fatigue limit in an air environment, the Rebinder theory would predict a similar limit in corrosion-fatigue. However, this prediction is not confirmed in corrosion-fatigue data, rather the corrosion-fatigue strength continues to decrease as the life increases. Therefore, each of the proposed mechanisms explains certain aspects of faster crack initiation in a corrosive environment; however, it is shown that none of them can single handedly explain the phenomena involved.

2.2 Trends in Fatigue of Low-alloy Steel in Various Environments

Fatigue has often been described as the number one cause of failure in engineering metals. When a corrosive environment is combined with fatigue loading, large decreases in the fatigue life of the metal are encountered. Outlined below are specific studies that demonstrate the general trends found when low-alloy steel is fatigued in air and aqueous salt solutions.

2.2.1 Fatigue of Steel in an Air Environment

In this section, the trends observed when a smooth steel specimen is fatigued in an air environment are investigated. Fatigue has been studied in steel for over 150 years since W.A.J. Albert conducted the first recorded study of metal fatigue in 1829 when he studied the failure of mine-hoist chains under bending type loading.[3] Since that time, many crack initiation and propagation theories have been presented that attempt to capture the behavior that is observed. A review of work relating to low-alloy steel in this context follows.

Fatigue cracks that lead to failure are observed to be a result of three constituents, cyclic stress, tensile stress, and plastic strain. If any one of these three is not present, a fatigue crack will not initiate or propagate.[6] Assuming these constituents are present, the first and most important step leading to failure is crack initiation. The cyclic deformation and crack initiation phases of fatigue tend to make up the majority (90% or more) of the life of most parts that are designed to last a high number of cycles, typically 100,000 cycles or more.[4]

The initiation of fatigue cracks in polycrystalline low-alloy steel in an air environment is most often found to result from inclusions, or surface defects. Cracks are most likely to initiate on the surface of a material rather than in the bulk section. A study conducted by Zhu et al. in 1986, showed that fatigue cracks initiated at mainly harder silicate inclusions located on the surface of AISI 4130 steel specimens when fatigued in an air environment.[7] Surface roughness caused by machining operations serves as stress concentrations that initiate into cracks. Therefore, in an air environment, inclusion content and surface roughness are very important to the fatigue life of steel.

One other site where cracks are known to initiate in metals is at persistent slip bands (PSB) where irreversible slip occurs and serves to concentrate dislocations into high strain zones. When these zones break the surface of the metal and create surface roughness, they become ideal crack initiation points. PSB are primarily observed in single crystal metals although researchers such as Pohl, Mayr, and Macherauch have observed PSB in the interior sections of fatigued polycrystalline low-carbon steel after cyclic loading.[3] Small PSB are also expected in large grains that are in contact with the surface; therefore, these bands are found to result in crack initiation even in polycrystalline materials.

Once cracks initiate and begin propagating at a stable rate, they are observed to propagate transgranularly. In a study by Tau et al., transgranular propagation with quasi-cleavage facets were observed in the fracture features of both bainitic and tempered martensitic AISI 4130 steels fatigued in an air environment.[8] This study showed that cracks propagate transgranularly in low-alloy steel regardless of microstructure.

Hardness, strength, and fatigue limit are closely related in steels. If a material is observed to have a high hardness, the strength and fatigue limit are also expected to be high. Research published by Breen, et al., in 1979 showed that increasing the hardness of AISI 4140 steel from 20 – 45 HRC increases the endurance limit of the steel. However, when the hardness is increased further from 45 – 50 HRC, the endurance limit declines.[6] This effect is observed in Figure 2.3. The cause for the drop-off endurance limit for the high hardness values was noted to be the residual stresses within the structure introduced by quenching and insufficient tempering temperatures. When steel is quenched, large

residual stresses are developed within the structure that tempering usually serves to reduce.

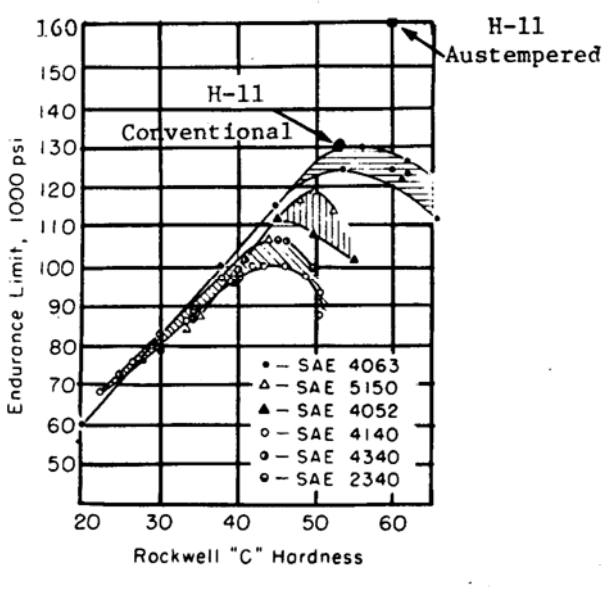

Figure 2.3. Relation of endurance limit to hardness of six alloy steels[6]

Microstructure can be used to explain some of the effects that are observed in the mechanical properties of low-alloy steel. One phase in particular that is important to this material is martensite. This phase is primarily responsible for the strength gains that are achieved from heat treatment. Figure 2.4 shows the fatigue limit of several compositions of steel as a function of martensite content. As seen in the graph, the fatigue limit is found to be highest when the martensite percentage is high. A tempered martensite structure is also observed to provide the highest fatigue limit of any structure found in this steel for an air environment.

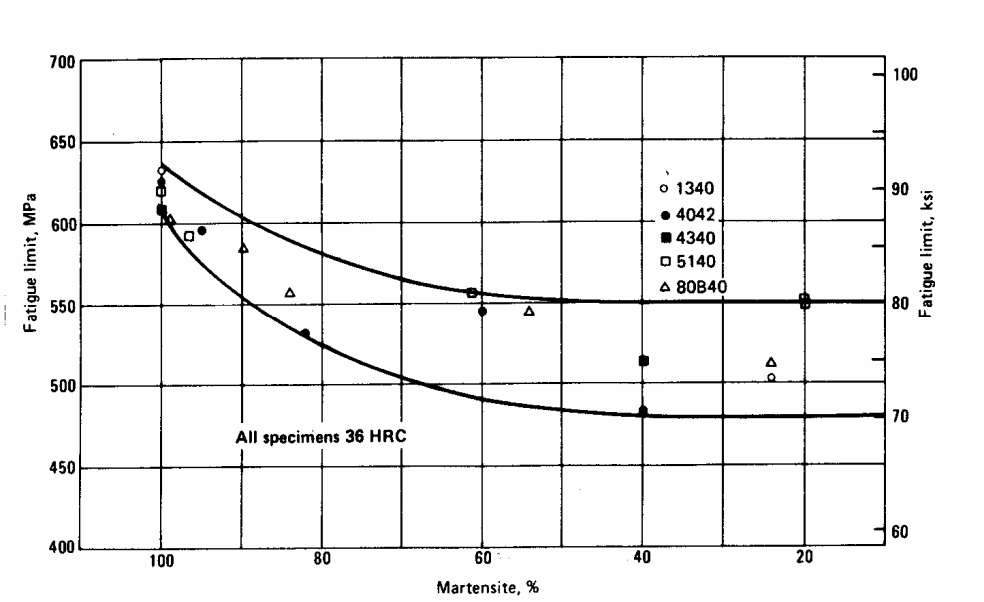

Figure 2.4. Medium-Carbon Alley Steels, Five Grades: Effect of Martensite Content[6]

2.2.2 Corrosion-fatigue of Steel in an Aqueous Salt Environment

The first trend to be noticed in corrosion-fatigue behavior is that the fatigue limit observed when steel is fatigued in air is significantly lower or erased by a corrosive environment. Figure 2.5 illustrates this general trend. As the figure illustrates, the fatigue strength of the metal in corrosive environment continues to fall as the cycles to failure is increased. It has been found that in most low-alloy steels fatigued in contact with salt solutions, there is no "safe stress range" at which the metal has infinite life.[6] These steels may be reported to exhibit an endurance limit at a specified number of cycles, but no true fatigue limit is observed.

A specific example of a corrosive environment lowering the fatigue limit of steel is found in the study conducted by Kitagawa on a fracture mechanics approach to corrosion-fatigue of un-notched specimens. In this study, the data originally reported by

McAdams in 1928 was represented as in Figure 2.6.[9] The graph shows the well-known relationship of fatigue strength to ultimate tensile strength in both an air and a corrosive environment. As seen in the figure, the fatigue limit increases linearly as the tensile strength increases, however the corrosion-fatigue limit is observed to stay constant and even decrease with increasing tensile strength. This study provides an excellent example of the effect of corrosive media on the fatigue limit of steel.

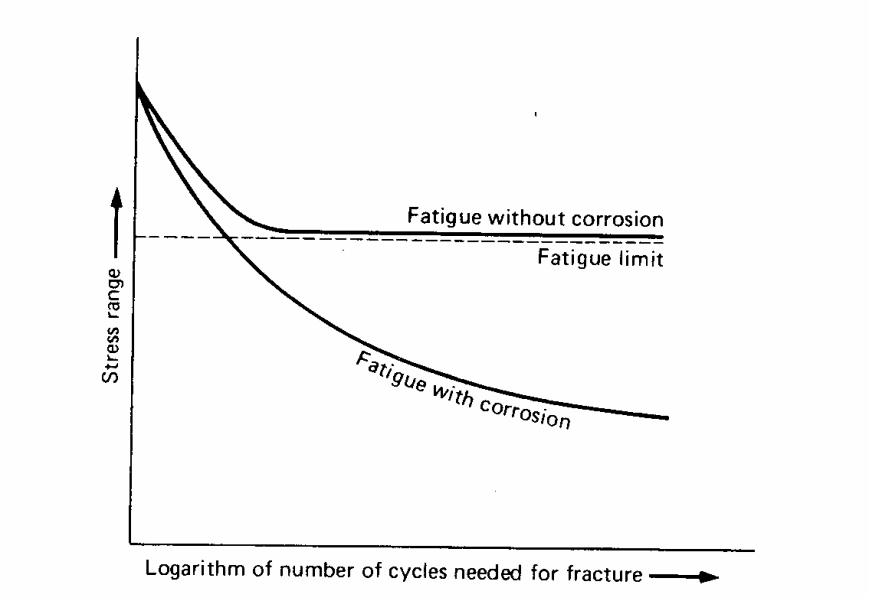

Figure 2.5. Corrosion-fatigue and its general effect on the behavior of steel [6]

The fact that most of the fatigue life of steel (90% or more) is spent initiating a crack means that any decrease in the time that it takes to initiate causes large losses in life of the material. Crack initiation is studied extensively as the main cause of decreased life of steel exposed to corrosive solutions. In 1983, Novak studied the corrosion-fatigue crack initiation (CFCI) behavior of four structural steels. The steels represented strength levels between 207 to 1034 MPa (30 to 150 ksi). Two of the steels were ferrite-pearlite

microstructure, and the other two were martensitic structure.[4] He sought to observe the differences in crack initiation behavior between the various strengths and microstructures represented.

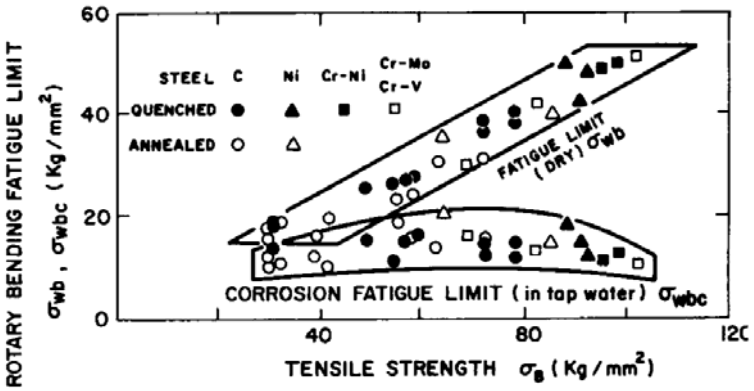

Figure 2.6. Relation of the fatigue limit to tensile strength in air and water[9]

The investigation by Novak provides several key points on the crack initiation behavior of steel. Despite the obvious differences in the strength and microstructure of the steels, the CFCI behaviors of each when exposed to 3.5% NaCl were virtually identical. This observation led to a conclusion that CFCI is insensitive to large changes in both strength and microstructure. These findings are also in agreement with those found in Figure 2.6. Novak also observed that there was no threshold value of stress at which the steels would experience infinite life. He concluded that the ferrite-pearlite and tempered martensite structures that were tested should not be used in structural applications when they are likely to be in contact with salt containing solutions.[4]

In Zhu's work on crack initiation and propagation in AISI 4130 steel exposed to perchlorate solution, he showed that a corrosive solution served to decrease the crack initiation life and total fatigue life compared to specimens tested in air. This effect was

observed as a result of the corrosion process altering the crack nucleation mechanism and accelerating the kinetics of failure. The crack initiation sites in air environment were inclusions, whereas the initiation sites in corrosive environment were at grain boundaries.[7] This work was done in perchlorate solution, but the general effects are seen in salt-water solution as well.

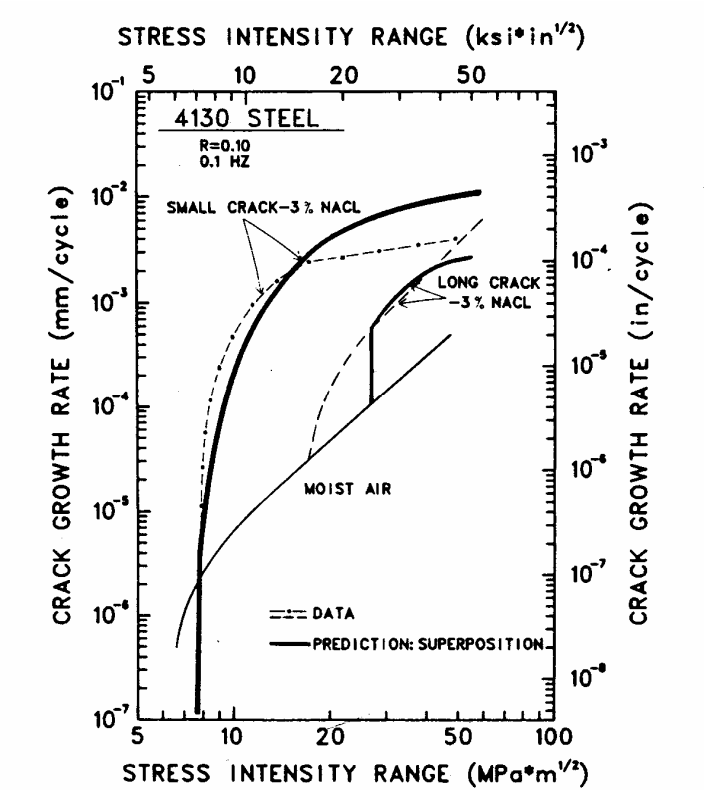

Figure 2.7. Corrosion-fatigue crack growth rates various environments[10]

In addition to faster initiation in a corrosive environment, the corrosion-fatigue life is also reduced by accelerated crack growth rates. As can be seen in Figure 2.7, the crack growth rate of AISI 4130 steel in 3% NaCl is consistently higher than the rate in moist air. The data that was originally reported by Gangloff is found in a study by McEvily.[10] Also, the rate is higher for short cracks over long cracks. Therefore, a crack in a salt-water environment is found to propagate more rapidly than a crack in air

environment. The small versus long crack variation is a result of the chemistry involved at an occluded crack tip. Small cracks tend to experience more active corrosion and subsequent faster rates of propagation.

Table 2.1. Heat treatment, hardness, yield strength for AISI 4130[8]

Symbol	Heat treatment (°C/min)*	Hardness HR_C	σ_{ys}(MPa)	K_{Ic}(MPa $m^{1/2}$)
TM350	austenized + WQ, tempered(350/60)	43.3	1218±18	90.4
TM450	austenized + WQ, tempered(450/60)	36.7	1015±5	125.1
TM600	austenized + WQ, tempered(600/60)	26.3	676±7	118.1
B330	austenized + SBQ(330/60)	40.2	1192±14	123.8
B370	austenized + SBQ(370/60)	35.2	1005±10	116.5
B470	austenized + SBQ(470/60)	21.4	647±3	80.2

*Austenized at 850°C for 30 min, WQ = water quench; SBQ = salt brine quench

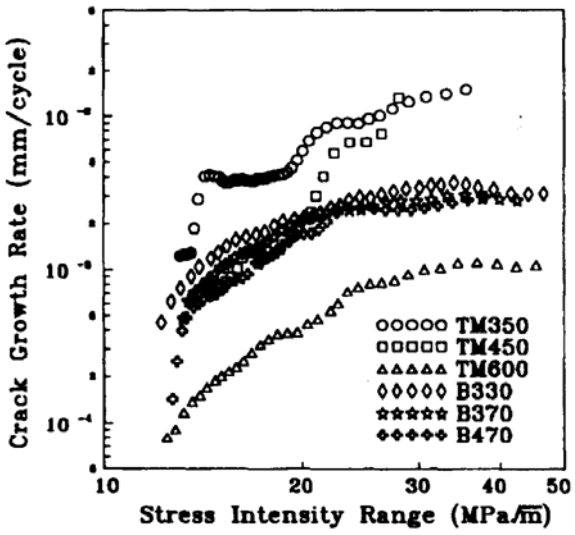

Figure 2.8. Log da/dN vs. log ΔK curve under hydrogen environment[8]

In a study by Tau, Chan, and Shin, it was demonstrated that as the yield strength of AISI 4130 steels is increased, higher fatigue crack propagation rates are obtained. The study also shows that high strength steels are sensitive to hydrogen embrittlement and hydrogen enhanced environmental fatigue crack propagation. Therefore, higher strength steels are expected to have higher rates of fatigue crack propagation when exposed to corrosive environments as compared to lower strengths. Table 2.1 and Figure 2.8

together show that higher strength levels result in higher corrosion fatigue crack propagation rates. Table 2.1 contains the heat treatment, hardness, and yield strength for various microstructures of AISI 4130 steel that were tested by Tau, et al. Figure 2.8 illustrates the results of fatigue crack growth rate in hydrogen charged environment.[8]

In addition to the traditional observation that corrosive environment decreases the fatigue life of steel, parameters have been discovered that affect the amount of this decrease. These parameters include cyclic frequency and load ratio (min load / max load). Increasing the cyclic frequency generally serves to decrease the effects of environment on fatigue lives.[11] In fact, crack retardation and stoppage in structural steel during constant amplitude fatigue have been observed when specimens were cycled at 10 Hz. Crack retardation was absent when the specimens were cycled at 1 Hz.[12] The retardation and stoppage of the crack was caused by corrosion product wedging that increased the amount of crack closure and led to slow or nonexistent crack growth.

The previous example represents an unlikely occurrence in most corrosion-fatigue situations. With lower loading frequencies, it is found that the time dependence of the corrosion reaction creates the effect of increasing crack initiation and propagation rates as the frequency is decreased. It is found that the longer the corrosive media is allowed to attack the material between loading events, the more damage that is done to progress the crack. The crack growth rate in absence of corrosion is insensitive to frequency of load application over a wide range of values.[13]

The load ratio or R-ratio is also very important in corrosion-fatigue because it determines the amount of mean stress applied to the specimen. Generally, higher R-ratios mean lower the fatigue strength at a given maximum stress.[14]

CHAPTER III

MATERIALS AND SPECIMENS

As previously stated, the material of interest in this research is AISI 4130 steel. The general characteristics of this material, test specimen geometry, heat treatment procedures, and specimen fabrication details are discussed in the following sections.

3.1 AISI 4130 Steel

The steel being investigated is known as ultra-high strength medium-carbon low-alloy steel.[15] In other publications such as the Metallic Materials Properties Development and Standardization (MMPDS) report, the material is also referred to as chromium-molybdenum steel.[16] This family of steels includes AISI 4130, 4140 and 4340 steels. Of the three, 4130 is the lower strength steel due to its lower carbon content. AISI 4130 has been accepted into general use because of its well-established heat-treatment procedures and processing techniques. In Table 3.1, the composition of this family of steels is listed for comparison.

Table 3.1. Chemical composition of three medium-carbon low-alloy steels[15]

Designation or trade name	Composition, weight %					
	C	Mn	Si	Cr	Ni	Mo
4130	0.28 - 0.33	0.40 - 0.60	0.20 - 0.35	0.80 - 1.10	…	0.15 - 0.25
4140	0.38 - 0.43	0.75 - 1.00	0.20 - 0.35	0.80 - 1.10	…	0.15 - 0.25
4340	0.38 - 0.43	0.60 - 0.80	0.20 - 0.35	0.70 - 0.90	1.65 - 2.00	0.20 - 0.30

AISI 4130 steel possesses low-to-intermediate hardenablility and can be heat-treated by solution annealing then quenching in water or oil followed by tempering. The

tempering treatment allows for the tensile strength and the fracture toughness to be set to desired values. Standard heat treatment temperatures and resulting mechanical properties for this particular steel are shown in Table 3.2.

Table 3.2. Mechanical properties and tempering temperatures for AISI 4130[15]

Tempering Temperature		Tensile Strength		Yield Strength		Elongation in 50 mm	Reduction in Area	Hardness
(C)	(F)	(MPa)	(ksi)	(MPa)	(ksi)	(%)	(%)	(HB)
205	400	1550	225	1340	195	11.0	38.0	450
260	500	1500	218	1275	185	11.5	40.0	440
315	600	1420	206	1210	175	12.5	43.0	418
370	700	1320	192	1120	162	14.5	48.0	385
425	800	1230	178	1030	150	16.5	54.0	360
540	1000	1030	150	840	122	20.0	60.0	305
650	1200	830	120	670	97	24.0	67.0	250
Note: 25 mm (1 in.) diameter bars oil quenched from 860 C (1575 F) and tempered 2 hours with air cool								

The typical microstructure of quenched and tempered AISI 4130 steel ranges from primarily martensite for high strength levels to a combination of tempered martensite, bainite, and cementite for lower strength levels. The as-quenched condition of this steel contains mostly martensite and some retained austenite. The steel is often tempered to remove some of the brittle martensitic structure and introduce other phases that are more ductile. This process serves to lower the strength but increase the fracture toughness of the material. As an example, the retained austenite converts to bainite if the tempering temperature is higher than 250 °C (482 °F), and at temperatures from 200 - 700 °C (392 – 1292 °F), cementite (Fe_3C) is formed from carbon rich precipitates.[17] Since many phases can co-exist in the material depending on the temperature of heat treatment, it is often hard to distinguish the precise microstructure of low-alloy steel.

3.2 Test Specimen Geometry

For the current project, a dog-bone type tensile specimen was selected for tensile, fatigue, and corrosion-fatigue testing. Goodyear Tire and Rubber Company supplied the

test material in the form of rectangular bars that measured approximately 4.5 x 25.4 x 0.64 cm (1.75 x 10 x 0.25 in.). Six specimens were machined from each bar. The layout of the specimens with respect to the test material is shown in Figure 3.1.

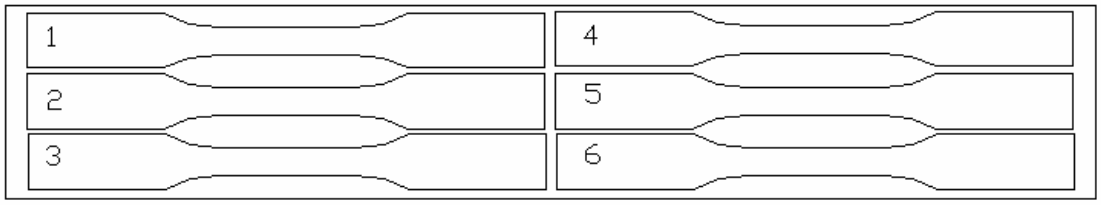

Figure 3.1. Specimen orientation with respect to test material

The dimensions of the test specimens are shown in Figure 3.2, and were identical for each type of testing. The specimen shape was determined from criteria found in ASTM E 8-03,[18] which is a standard for tension testing metallic materials. In addition, the corners of the square gage section were rounded slightly to reduce the stress concentration in that area primarily to mitigate the risk of starting fatigue cracks from the corners.

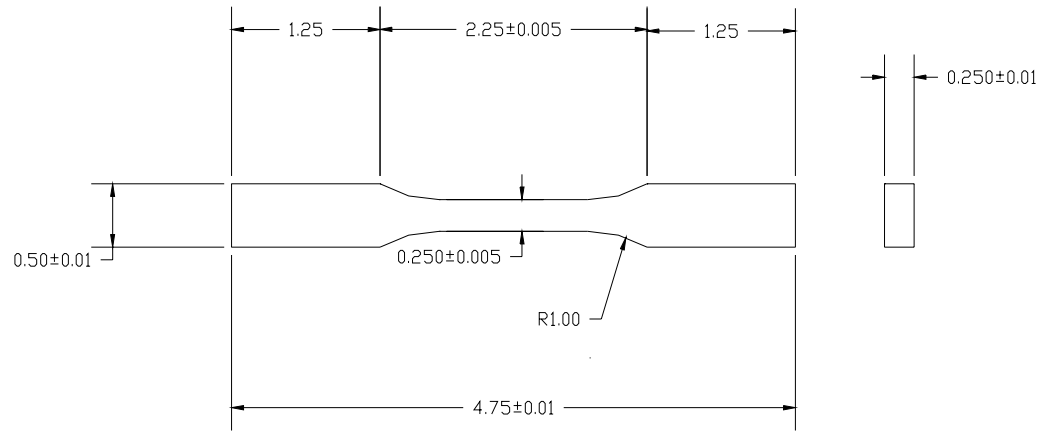

Figure 3.2. Specimen geometry used for tensile, fatigue, and corrosion-fatigue testing (dimensions in inches)

3.3 Specimen Heat Treatment and Fabrication

Due to the large number of specimens needed for this project and the relative hardness of the material, the heat treatment and fabrication were performed by outside vendors who were specially equipped to handle such quantities of material and maintain consistency during the heat treatment and subsequent machining. Details of the heat treatment and machining of the specimens are described in the following sections.

3.3.1 Heat Treatment

The material was divided into six batches that were heat treated separately. The batches designated A, B, and D were sent to Bodycote Thermal Processing in Cincinnati, Ohio for heat treatment. The remaining three batches, C, E, and F, were heat treated by Braddock Metallurgical in Atlanta, Georgia. Batches B & C, and D & E were repeat heat treatments so that more specimens could be obtained in the medium strength level.

Table 3.3. Heat treatment temperatures and corresponding hardness values

Batch Letter	Tempering Temperature (2 hrs, air cooled)		Desired Hardness (HRC)	Desired Hardness (HB)
	(C)	(F)		
A	704	1300	24.0	250
B	593	1100	27.0	271
C	593	1100	27.0	271
D	482	900	38.0	362
E	482	900	38.0	362
F	205	400	48.0	444

The two heat treatment facilities followed roughly the same procedure when processing the material. The bars were heated to 871 °C (1600 °F) for one hour then oil quenched. Following quenching, the bars were tempered for two hours at the temperatures shown in Table 3.3 to develop a range of strengths. Duplicate heat

treatments for the 27 and 38 HRC hardness levels were desired so that medium strength levels of this steel could be studied in more detail than the extremes. Heat treatments A and F represent the extremes of hardness in this steel. Hardness tests were conducted to determine if the heat treatments were successful.

3.3.2 Specimen Fabrication

After undergoing heat treatment, the steel bars were machined to the dimensions illustrated in Figure 3.2 by Cincinnati Testing Labs (CTL) in Cincinnati, Ohio. The machining procedures employed by CTL have passed both SAE AS7101 and ISO17025 inspections. The following steps were taken to machine the specimens.

a. Layout and punch the identification code on specimens
b. Blank specimens using abrasive saw
c. Finish grind width and length
d. Low stress grind thickness to a 32 RMS surface finish
e. Rough machine gage sections
f. Dress wheel and low stress grind gage sections
g. Polish gage sections to a 8 RMS surface finish
h. Inspect dimensions and tolerances per supplied drawings (Figure 3.2)

The machining marks left from the grind and polish steps ran in the longitudinal direction along the specimens to minimize the effects of machining on the fatigue properties being measured. Finally, the edges of the gage section of the specimens were rounded at a radius of approximately 0.635 mm (0.025 in.) to lower the stress concentration caused by the sharp edges of the square cross section. A total of 55 specimens, each machined to the same specifications, were prepared for testing.

CHAPTER IV

EXPERIMENTAL EQUIPMENT AND PROCEDURES

The following chapter discusses the mechanical testing methods employed to characterize the material described in Chapter III. The experimental equipment and procedures are discussed for hardness, tensile, and fatigue tests.

4.1 Hardness Testing

Since hardness tests are easily completed and relatively nondestructive, they are often used as first estimates of strength. In this project, hardness testing was accomplished through the Rockwell hardness testing method to determine if heat treatment was applied properly and to obtain an approximation of the strength of the material. The equipment and procedure for hardness testing is included below.

4.1.1 Hardness Testing Equipment

The hardness tester was a Leco FR-1E machine manufactured by Future Tech Corp. The device measures Rockwell hardness, and after being manually preloaded, it automatically provides a digital readout of the hardness.

A Leco brand "C" type indenter was used for testing. It is a diamond type indenter that is applied at a total test load of 1471 N or 150 kgf. This type of indenter and test load is recommended for steel, hard cast iron, titanium, and other hard metals.

A Rockwell hardness test block was employed to calibrate the machine prior to testing the actual samples. The test block was manufactured and standardized by Leco in accordance with ASTM E 18-03.[19]

4.1.2 Hardness Testing Procedure

The hardness testing procedure used in this research was derived from ASTM E 18-03[19] and the documentation provided with the machine. Following the standard, the device was calibrated on a test block of known hardness to ensure the tester was providing accurate readings. Following calibration, three hardness tests were completed on each specimen and the results were averaged to obtain a representative value. Specimens were indented on the grip section to prevent damaging the gage section.

4.2 Tensile Testing

Tensile tests are used to measure basic mechanical properties such as ultimate stress, yield stress, percent reduction in area, and percent elongation. To accomplish the objective of the project, accurate values for the tensile and yield strength of each heat treatment were necessary. The reduction in area and percent elongation values were also relevant in assessing the ductility, which is related to the toughness of the material.

4.2.1 Tensile Testing Equipment

An MTI Phoenix screw driven load frame and a twenty thousand pound MTI Load cell were utilized to test tensile properties. Instron 2716-003 wedge action grips with a capacity of 98.1 kN (22,500 lbf) secured the specimen. The elongation was measured by an MTS Model 632.11E-23 extensometer. The extensometer had a 2.54 cm (1.000 in.) gage length, and an extension range of +0.508 / -0.254 cm (+0.200 / -0.100 in.). The load, crosshead displacement, time, and extensometer displacement were recorded by an MTI digital data acquisition card connected to a personal computer containing MTI software.

4.2.2 Tensile Testing Procedure

The testing procedure used in this research was derived from ASTM E 8-03,[18] which covers the tensile testing of metals at room temperature. After calibrating the machine and setting up software to record the relevant data, the specimen was mounted in the wedge grips and secured in place. Double-sided tape was applied to the gage section where the extensometer contacts the specimen to prevent cracking at the contacts. The extensometer was then secured into place with rubber bands. The specimen was strained at a rate of 0.254 cm/min (0.1 in./min) until the measured strain reached 15%. At this point, the extensometer was removed to avoid damage due to overextension and the test was continued to failure.

The elongation reading from the extensometer was used to generate the stress-strain curve until it was removed at 15% strain. After this point, the curve was determined using the elongation obtained from crosshead displacement. The latter process assumed that in past yielding most of the deformation and therefore machine displacement consists of deformation localized in the gage length. The yield and ultimate tensile strengths were then calculated from the stress-strain curve. Measurements of the broken specimens were used to determine percent elongation and percent reduction in area.

4.3 Fatigue Testing in Air Environment

Fatigue tests required different equipment than tensile tests because of the requirement for dynamic loads. Since it is well known that fatigue in air is not significantly dependent on frequency, load frequencies of up to 10 Hz were applied in the

air environment. Higher frequency loading was desired to reduce the time required to conduct these tests.

4.3.1 Fatigue Testing Equipment

A 97.9 kN (22,000 lbf) hydraulically actuated MTS 312.21 load frame and accompanying MTS 661.21A load cell were used to fatigue the specimens. An MTS Teststar IIs workstation link connected the test equipment to a personal computer containing MTS Teststar software. The function generator contained in the software controlled the loading, wave shape, and cycle count required for these tests. Because the specimen was identical for tensile and fatigue tests, the Instron 2716-003 wedge action grips were used in both tests.

4.3.2 Fatigue Testing Procedure

The fatigue testing procedure was similar to that found in ASTM 466-96.[20] This document identifies the standard practice for conducting force controlled constant amplitude axial fatigue tests of metallic materials. The standard is used to obtain fatigue strength of metallic materials in the fatigue regime where strains are primarily elastic. What follows are the details of these tests.

Prior to testing, the wedge type grips and the specimen within the grips were visually aligned in the loading direction to promote only axial stresses in the gage section. Strain gages were not used in fatigue tests because later testing involved submersion in corrosive fluid. The parameters that were recorded for each fatigue test included the maximum and minimum axial force and cycles to failure. Test frequency was most often set at 10 Hz, and failure was defined by complete separation of the

specimen. The number of cycles until run-out was set at 10^6 cycles although some specimens were fatigued beyond that as time permitted. The stress ratio (ratio of minimum stress to the maximum stress in the loading cycle) was constant for each test at a value of R = 0.1. The test environment consisted of laboratory air at an average temperature of approximately 20 °C (68 °F). A triangular wave shape was chosen for the forcing function consisting of load versus time. Table 4.1 shows the test matrix used for fatigue testing in air environment.

Table 4.1. Test matrix for fatigue tests in air environment

Number of Tests (#)	Batch Letters	Load		Approx. Stress		Loading Frequency (Hz)	Environment
		Max (kgf)	Min (kgf)	Max (MPa)	Min (MPa)		
1	A	2449	245	596	60	10	air
1	A	2812	281	684	68	10	air
2	A, B	2948	295	717	72	10	air
1	B	3039	304	739	74	10	air
2	C, D	3139	314	763	76	10	air
1	D	3765	376	916	92	10	air
1	D	3856	386	938	94	10	air
1	D	3992	399	971	97	10	air
2	E	4082	408	993	99	10	air
1	F	4082	408	993	99	10	air

4.4 Corrosion-fatigue Testing

For the corrosion-fatigue tests, the gage section of the specimen was submerged in a salt solution while the specimen was fatigued. The following sections detail the equipment and procedures that were employed in these tests.

4.4.1 Corrosion-fatigue and Fluid Supply Equipment

Fatigue in the corrosive environment was completed with the same equipment used in the air fatigue tests with the addition of a corrosion chamber, a fluid supply

system, and the corrosive fluid. The corrosion chamber was specifically designed for this testing since there was no chamber readily available to test a tensile type specimen. A Julabo C-5B/3 fluid pump/heater was utilized to provide a fresh supply of corrosive fluid to the specimen. The heater function of the device was not used during testing. A Second Nature brand air pump supplied laboratory air to the fluid reservoir through a diffuser ball. This action provided constant oxygen content in the solution. The corrosion-fatigue setup can be seen in schematic form in Figure 4.1.

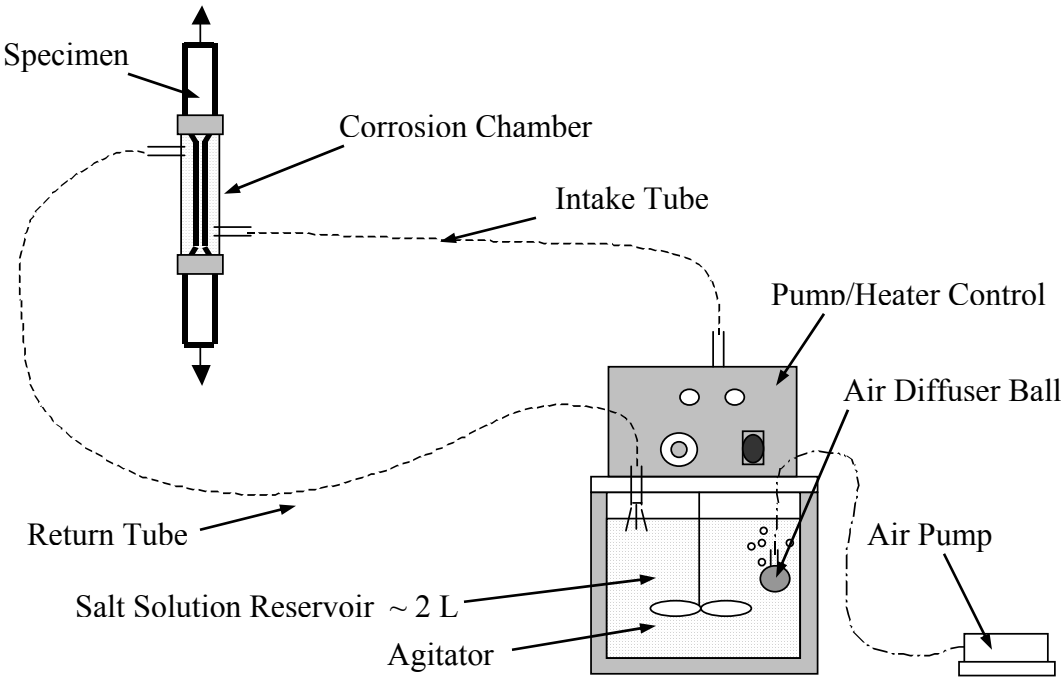

Figure 4.1. Diagram of the corrosion-fatigue testing equipment

As mentioned, a specially designed corrosion chamber was required to test the tensile type specimens of this project. A picture of the chamber is shown in Figure 4.2. The design requirements were that it be completely watertight, fully surround the gage section of the specimen, and provide a fresh supply of fluid to the specimen for the length

of a fatigue test. To fill these requirements, a cylindrical clear plastic tube with an outer diameter of 19 mm (3/4 in.), a wall thickness of approximately 0.66 mm (0.026 in.), and a length of 51 mm (2 in.) was fitted with rubber caps. The ends of the caps were cut to allow the specimen to slide through the chamber. In this way, the specimen could protrude through both ends of the chamber and the chamber would surround the gage section. Holes were drilled in the sides of the plastic cylinder so that the intake and return tubes could be attached. The intake tube had a 5.5 mm (0.22 in.) outer diameter and a 0.75 mm (0.03 in.) wall thickness. The return tube was larger to ensure that the fluid would flow without pressure buildup in the chamber. The return tube had a 9.52 mm (3/8 in.) outer diameter and a 1.59 mm (1/16 in.) wall thickness. After fitting of the assembly was complete, the caps and tubes were sealed into place using silicone household glue manufactured by GE. The glue was 100% silicone and provided a durable and watertight seal.

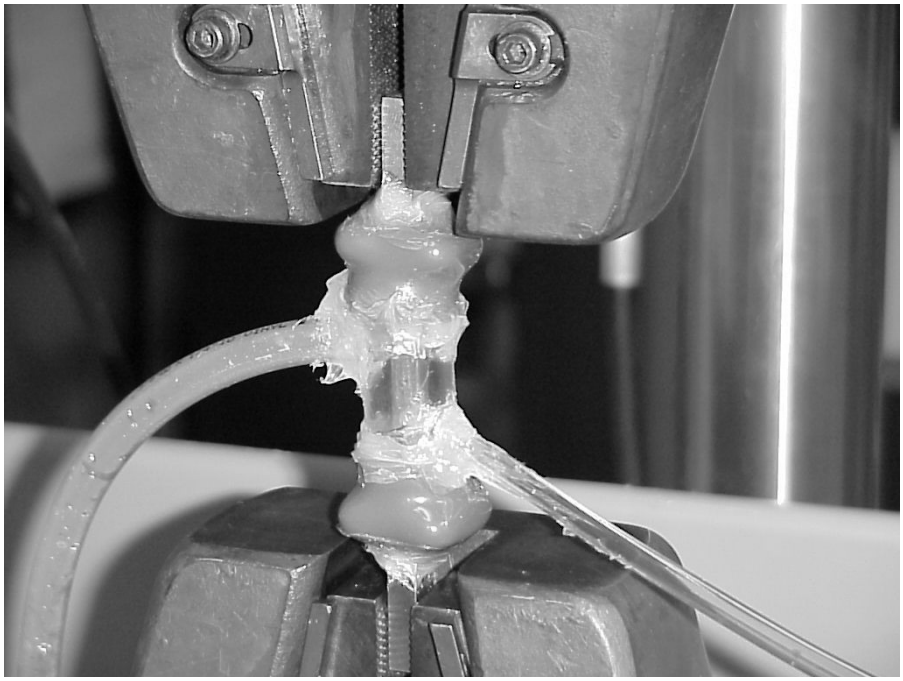

Figure 4.2. Picture of the corrosion chamber designed for this project

The salt solution was prepared as prescribed by SAE J2334,[21] which is a cosmetic corrosion lab testing procedure. This standard was selected because the aqueous salt solution it describes is believed to provide excellent correlation to severe corrosive field environments.

The solution contains a mixture of the following three salts dissolved in DI water on a weight percent basis:

1. 0.5% NaCl
2. 0.1% $CaCl_2$
3. 0.075% $NaHCO_3$

According to the standard, the pH of the solution must be measured and recorded prior to testing and on a weekly basis thereafter. The pH measurement was taken using an Alkacid Test Ribbon manufactured by Fisher Scientific Company. The average pH of the solution was determined to be around 8. If the pH varied by more than one in either direction, the batch of solution was discarded, and a new batch was mixed.

4.4.2 Corrosion-fatigue Testing Procedure

The procedure employed for corrosion-fatigue tests was similar to that found in Section 4.3.2. The parameters that are common between the two test programs include loading, failure criteria, stress ratio, temperature, and wave shape. Test environment and loading frequency were the only differences. The test environment for the specimen was total immersion in the salt solution described in the previous section, and the test frequency was set at 1 Hz so that the effects of the corrosive environment would be apparent.

In preparation for testing, the following procedure was followed. The corrosion chamber was attached to the gage section using the same silicone adhesive described in the previous section. This step was completed at least 24 hours before each test to ensure the silicone was cured before the solution was pumped through. After the silicone was cured, the specimen was loaded into the machine and the input and return tubes of the chamber were attached to the pump apparatus. The reservoir was then filled with solution and the pH checked to ensure it was around 8. The pump was then turned on and fluid flowed through the chamber. The testing software was set to complete the fatigue test and the test ran until the specimen fractured. At fracture, the maximum and minimum force applied and the cycles to failure were recorded. Table 4.2 includes the test matrix used in corrosion-fatigue testing.

Table 4.2. Test matrix for corrosion-fatigue tests in salt solution

Number of Tests (#)	Batch Letters	Load		Approx. Stress		Loading Frequency (Hz)	Environment
		Max (kgf)	Min (kgf)	Max (MPa)	Min (MPa)		
2	A, E	2132	213	518	52	1	corrosive
1	A	2449	245	596	60	1	corrosive
2	C	2631	263	640	64	1	corrosive
1	A	2812	281	684	68	1	corrosive
2	A, B	2948	295	717	72	1	corrosive
2	B, D	3039	304	739	74	1	corrosive
1	C, E	3139	314	763	76	1	corrosive
1	D	3583	358	871	87	1	corrosive
1	D	3856	386	938	94	1	corrosive
1	D	3992	399	971	97	1	corrosive
3	E	4082	408	993	99	1	corrosive
3	F	4082	408	993	99	1	corrosive

CHAPTER V

RESULTS AND DISCUSSION

Hardness, tensile, fatigue, and corrosion-fatigue test data were obtained by the procedures outlined in Chapter IV. Results from these tests are included in the following sections. Notable trends and analysis of the data are included in the discussion section of this chapter.

5.1 Hardness Test and Heat Treatment Results

The tempering temperature and desired hardness for each batch of material was previously presented in Table 3.3. To verify consistency during processing, the hardness of each machined specimen was tested. The results of the tests are shown graphically in Figure 5.1. The error bars in the graph show plus and minus one standard deviation in the data.

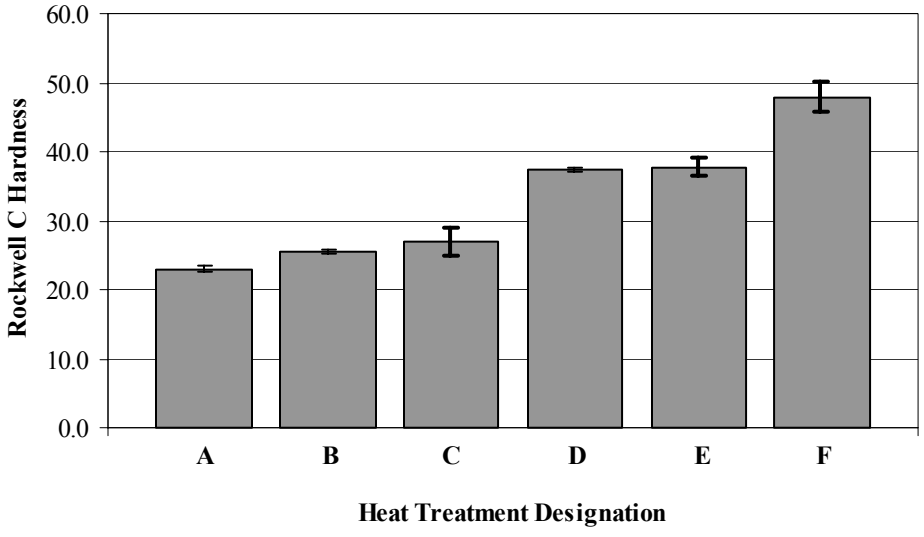

Figure 5.1. Average hardness values and standard deviation for each heat treatment

The desired and measured hardness values were compared and the result is shown in Table 5.1. It was found that even though heat treatments B and C were processed through different vendors, their respective hardness varied less than 6% from the desired value. In the case of heat treatments D and E, the variation from the desired hardness was less than 1.5%. Based on these results and the others found in Table 5.1, it was concluded that the heat treatments were satisfactory for the project.

Table 5.1. Comparison of desired and measured hardness values

Batch Letter	Desired Hardness (HRC)	Measured Hardness (HRC)	Percent Difference (%)
A	24.0	23.0	4.3%
B	27.0	25.5	5.7%
C	27.0	26.9	0.4%
D	38.0	37.5	1.3%
E	38.0	37.8	0.5%
F	48.0	48.0	0.0%

5.2 Tensile Test Results

Tensile tests were conducted on two specimens from each heat treatment batch except batch B where only one specimen was tested. The ultimate tensile strength, 0.2% offset yield strength, reduction in area, and percent elongation are reported in Table 5.2. Where it is appropriate, each result is the average value from two tests.

Table 5.2. Tensile test results organized by heat treatment batch

Measurement	Units	Heat Treatment Batch					
		A	B	C	D	E	F
Ult. Tensile Strength	MPa (ksi)	837 (121)	888 (129)	964 (140)	1215 (176)	1296 (188)	1846 (268)
0.2% Yield Strength	MPa (ksi)	736 (107)	813 (118)	823 (119)	1167 (169)	1229 (178)	1307 (189)
Reduction in Area	%	60.4%	61.1%	60.9%	55.4%	50.4%	44.5%
Elongation in 25 mm (1 in.)	%	25.2%	23.8%	18.7%	13.7%	13.5%	12.4%

5.3 Fatigue Results from Tests Conducted in Air

High cycle fatigue results are most often represented in the form of an S-N diagram where the maximum stress, minimum stress, or stress amplitude is plotted versus the cycles to failure. In the results discussed below, the maximum stress is plotted on a linear scale while the cycles to failure is plotted on a logarithmic scale. For each test, the stress ratio (minimum stress divided by maximum stress) was constant at 0.1. Figure 5.2 summarizes the data from the fatigue tests in laboratory air. Arrows on data points indicate run-outs.

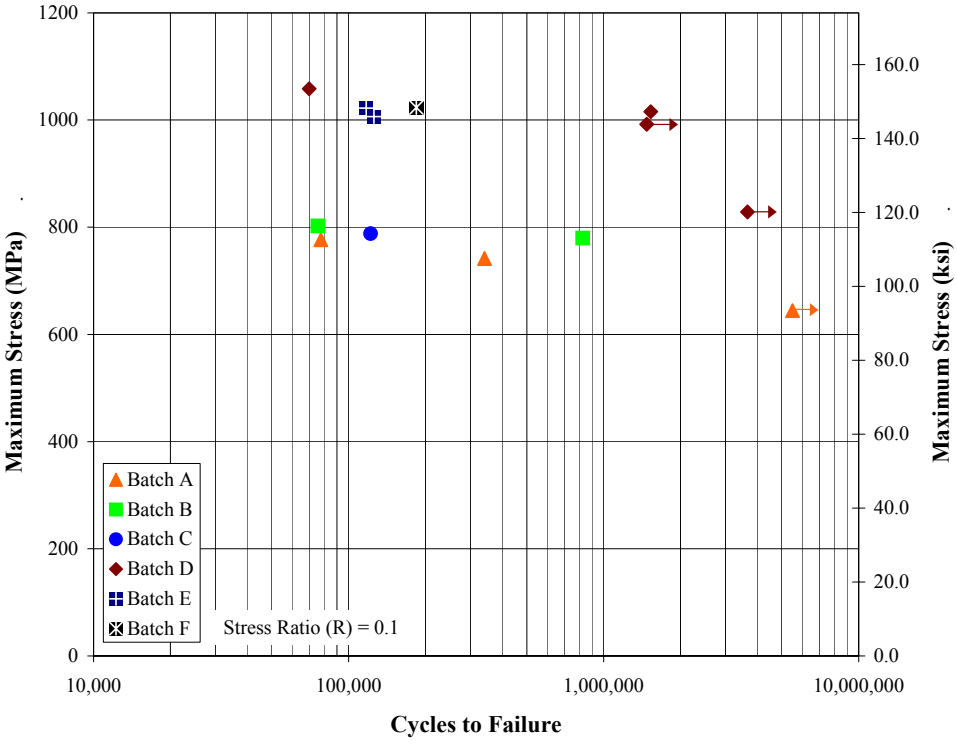

Figure 5.2. Fatigue test results for a laboratory air environment for the AISI 4130 steel at various strength levels. All tests were conducted at a stress ratio, R, of 0.1.

The data illustrated in Figure 5.2 is included in Table 5.3 along with other important test parameters. The table shows frequency of loading, maximum applied

stress, and maximum stress normalized by the yield and ultimate tensile strengths. Run-outs were obtained from batch A when the maximum applied stress was less than this batch's yield stress. Therefore, the maximum applied stress was set above the yield strength in order to avoid run-out.

Table 5.3. Fatigue data from tests conducted in a laboratory air environment

Specimen Designation	Frequency	Max. Stress (R = 0.1)		Stress Mean/Ampltude		Cycles to Failure	Max. Stress / Yield (%)	Max. Stress / UTS (%)
	(Hz)	(MPa)	(ksi)	Sm (MPa)	Sa (MPa)			
A-3	10	647	94	354	290	5,500,000 R/O	88%	77%
A-4	10	741	108	407	334	341,347	101%	89%
A-5	10	777	113	427	350	77,843	106%	93%
B-2	10	780	113	429	351	828,156	96%	88%
B-3	10	802	116	441	361	75,955	99%	90%
C2-5	20	788	114	433	355	122,064	96%	82%
D-3	10	1016	147	559	457	1,529,085	87%	84%
D-4	10	828	120	456	373	3,665,881 R/O	71%	68%
D-5	10	1058	153	582	476	70,105	91%	87%
E1-3	1	1022	148	575	447	117,165	83%	79%
E2-5	10	1006	146	554	453	125,559	82%	78%
F1-3	1	1023	148	571	453	184,398	78%	55%

5.4 Corrosion-fatigue Test Results

Results from fatigue tests conducted in the aqueous salt environment are presented in Figure 5.3. The abscissa of the graph is plotted on a smaller scale than the previous results because of the smaller range of cycles to failure in this environment. As seen in the figure, each specimen failed in less than 150,000 cycles. It is also observed that the corrosion-fatigue data points are much closer grouped than the fatigue data generated in the air environment.

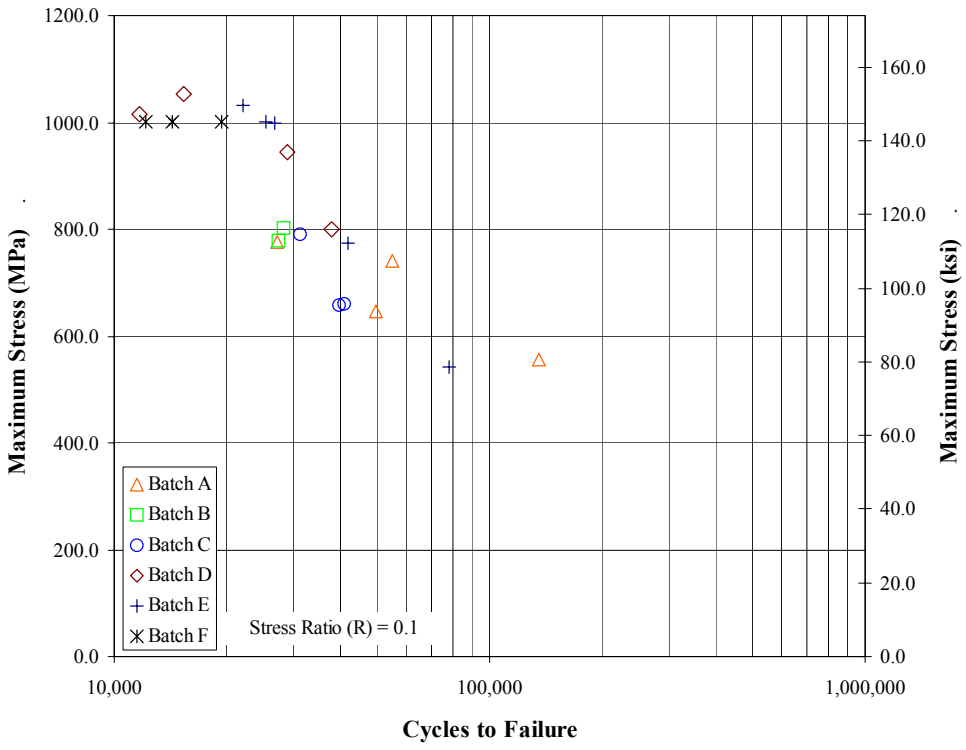

Figure 5.3. Fatigue test results from tests conducted in an aqueous salt environment for the AISI 4130 steel at various strength levels. All tests were conducted at a stress ratio, R, of 0.1.

The data points shown in Figure 5.3 are presented in Table 5.4 along with other significant information. The table shows that all tests were run at 1 Hz in the corrosive environment. This frequency was chosen to allow significant effects of corrosion-fatigue.

To allow easy comparison of the fatigue results from the air and corrosive environments, Figure 5.4 was constructed. In this graph, the solid symbols designate the data obtained from fatigue tests completed in the air environment, and the hollow symbols denote corrosion-fatigue data. As a general trend, the corrosion-fatigue data is grouped on the left portion of the graph.

Table 5.4. Fatigue results from tests conducted in aqueous salt environment

Specimen Designation	Frequency	Max. Stress (R = 0.1)		Stress Mean/Ampltude		Cycles to Failure	Max. Stress/ Yield (%)	Max. Stress / UTS (%)
	(Hz)	(MPa)	(ksi)	Sm (MPa)	Sa (MPa)			
A-6	1	645	94	355	290	49,921	88%	77%
A-7	1	741	107	407	333	54,918	101%	88%
A-8	1	777	113	428	350	27,102	106%	93%
B-4	1	778	113	428	250	27,413	96%	88%
B-5	1	803	116	442	361	28,324	99%	90%
C2-3	1	660	96	363	297	40,998	80%	68%
C2-4	1	658	96	362	296	41,271	80%	68%
C2-6	1	791	115	435	356	31,223	96%	82%
D-6	1	801	116	441	360	38,013	69%	66%
D-7	1	1016	147	559	457	11,647	87%	84%
D-8	1	1054	153	580	474	15,327	90%	87%
D-9	1	944	137	519	425	28,945	81%	78%
E1-4	1	1032	150	575	457	21,979	84%	80%
E2-1	1	1001	145	557	445	25,264	82%	77%
E2-2	1	999	145	556	443	26,781	81%	77%
E2-6	1	773	112	425	348	41,914	63%	60%
F2-1	1	1002	145	558	444	14,270	77%	54%
F2-2	1	1001	145	557	444	19,365	77%	54%
F2-3	1	1001	145	557	444	12,180	77%	54%

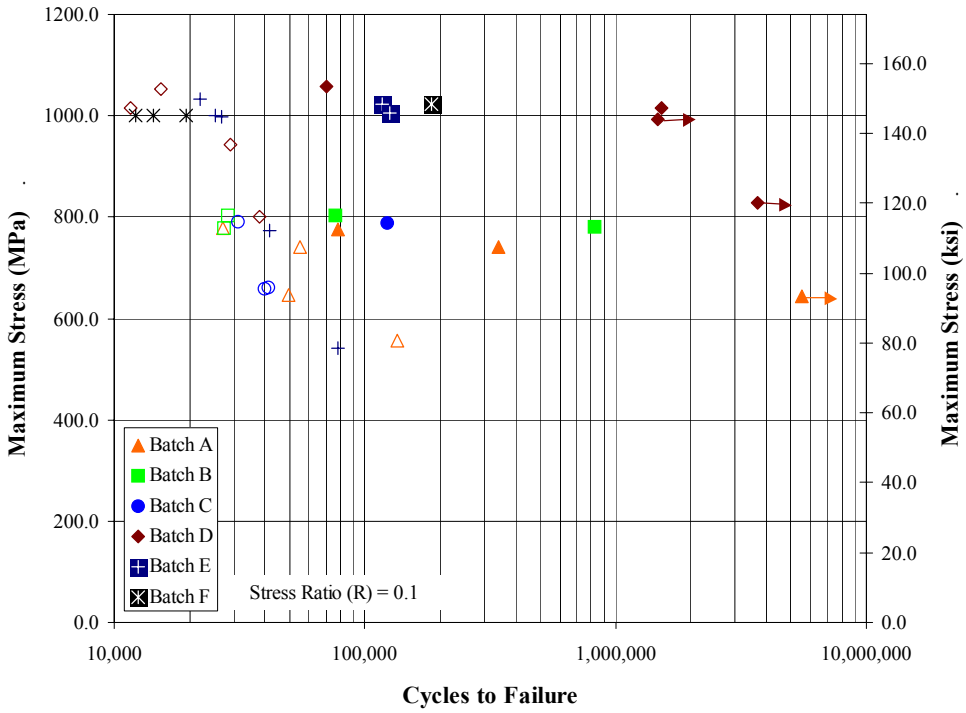

Figure 5.4. Combined fatigue results

Solid and hollow symbols represent fatigue in air and aqueous salt, respectively. All tests were conducted at a stress ratio, R, of 0.1.

5.5 Microscopic Examinations

In an attempt to explain the trends in the test results, the microstructure and fracture surface of several specimens were examined. The microstructure was studied to attempt to identify a particular phase that caused the effects in the fatigue behavior. The fracture surface was investigated to determine the type of cracking that led to failure. General observations are described in this section, and the interpretations of these observations are included in the discussion section.

5.5.1 Material Microstructure

As was discussed in Section 3.1, heat treatment directly affects the microstructure of steel and the microstructure, in turn, affects mechanical properties such as hardness, tensile strength, and fatigue strength. In this section, microstructural features will be examined and in the discussion section connections will be drawn between test results and microstructure.

Representative samples from heat treatment batches C, E, and F were extracted, mounted, polished, and etched to reveal their microstructure. An optical microscope attached to a personal computer was then used to produce digital pictures of the etched surface. These particular batches were selected because of the range of strength levels that they represent.

Batch C was chosen because of its medium to low strength level. This batch demonstrates the typical microstructure of the steel tempered to around 964 MPa (140 ksi). The structure of this batch is shown in Figure 5.5. The picture was taken at 50X magnification. Bainite, cementite, and tempered martensite are all expected at this strength level and evidence of their presence is seen in the picture.

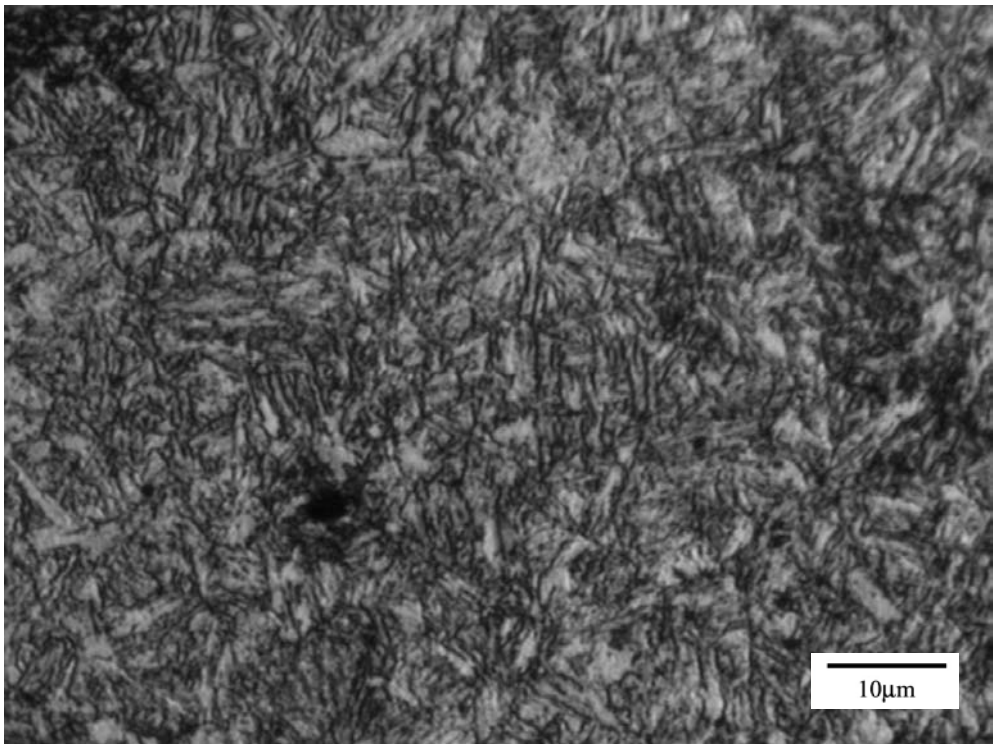

Figure 5.5. Microstructure of 964 MPa UTS specimen from batch C at 50X mag.

The microstructure of batch E was investigated to obtain the typical microstructure of high strength AISI 4130 steel. The tensile strength of batch E was 1296 MPa (188 ksi). The microstructure of batch E is shown in Figure 5.6 and is similar to that of batch C except that there is a higher percentage of tempered martensite present.

Batch F represented the highest strength investigated in this project. At an ultimate tensile strength of 1846 MPa (268 ksi), this batch can be labeled as an ultra-high strength level. The microstructure of batch F is shown in Figure 5.7. The tempered martensite surrounded by retained austenite structure closely resembles the 'as-quenched' condition in this steel. Some cementite was also found in the structure but the tempering temperature was not sufficient to convert the retained austenite to bainite.

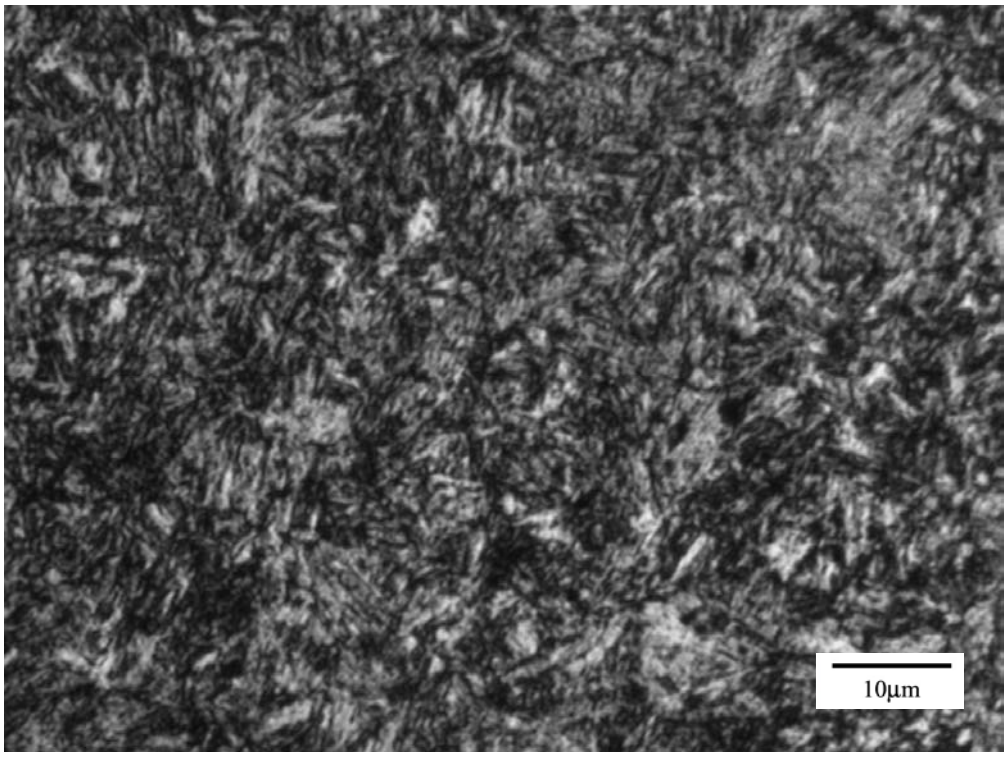

Figure 5.6. Microstructure of 1296 MPa UTS specimen from batch E at 50X mag.

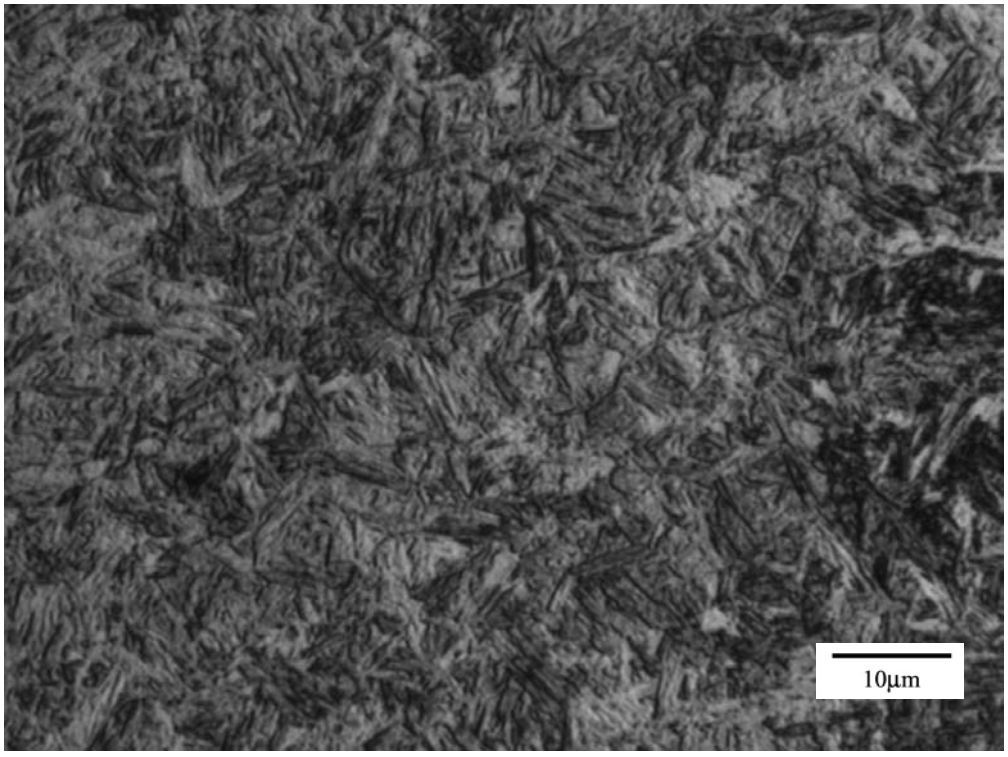

Figure 5.7. Microstructure of 1846 MPa UTS specimen from batch F at 50X mag.

5.5.2 Fracture Surface

The fracture surfaces of failed specimens were studied under the scanning electron microscope (SEM) to determine the type of cracking that was present and when and where in the microstructure the fatigue cracks initiated. The failed specimens that were studied were from the same three batches used in the investigation of the microstructure, C, E, and F. Two specimens from each batch were examined, one taken from a fatigue test in air environment and one from a corrosion-fatigue test. Photomicrographs were taken of the surfaces at a magnification of 1000X and were compared to determine the effects of different environments on the cracking behavior.

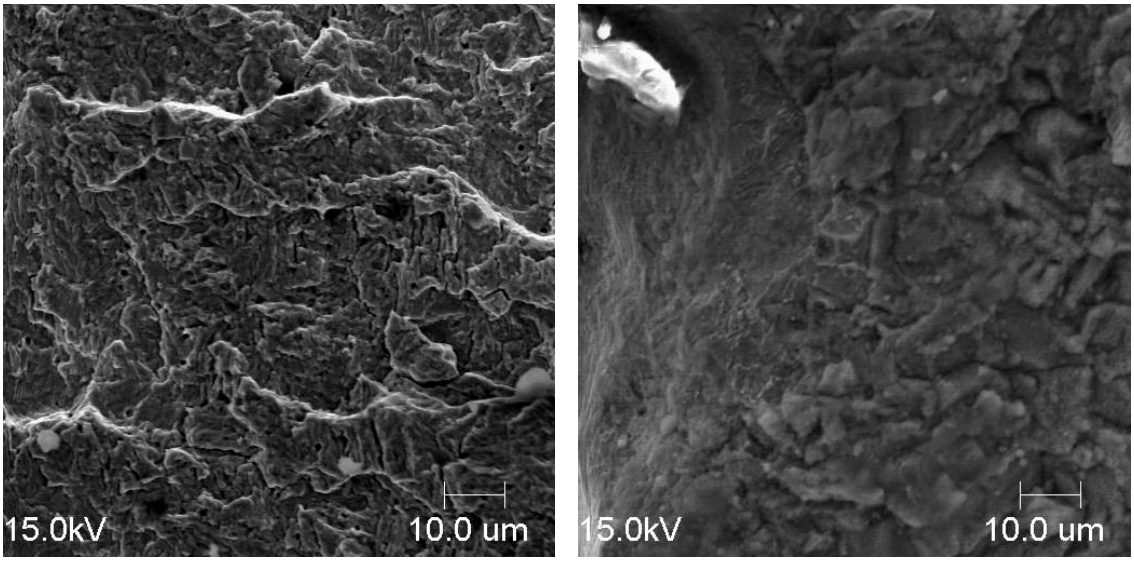

Figure 5.8. Fracture surfaces from batch C
Left: Specimen C2-5 fracture surface (air environment),
Right: Specimen C2-6 fracture surface (aqueous salt environment)

The specimens that were selected from batch C were C2-5 and C2-6. These specimens were both tested at a maximum stress of 790 MPa (115 ksi) with an R-value of 0.1. Specimen C2-5 was fatigued in an air environment and experienced 122,064 cycles

to failure. Specimen C2-6 was exposed to corrosion-fatigue and experienced 31,223 cycles to failure. Figure 5.8 shows a comparison of the two surfaces.

The two specimens from batch E, E1-3 and E2-2, were fatigued in air and aqueous salt environments, respectively. The maximum fatigue stress applied was approximately 1000 MPa (145 ksi) with an R-value of 0.1. Specimen E1-3 failed in 117,165 cycles while specimen E2-2 failed in 26,781 cycles. The SEM pictures of the fracture surface of both specimens are shown in Figure 5.9.

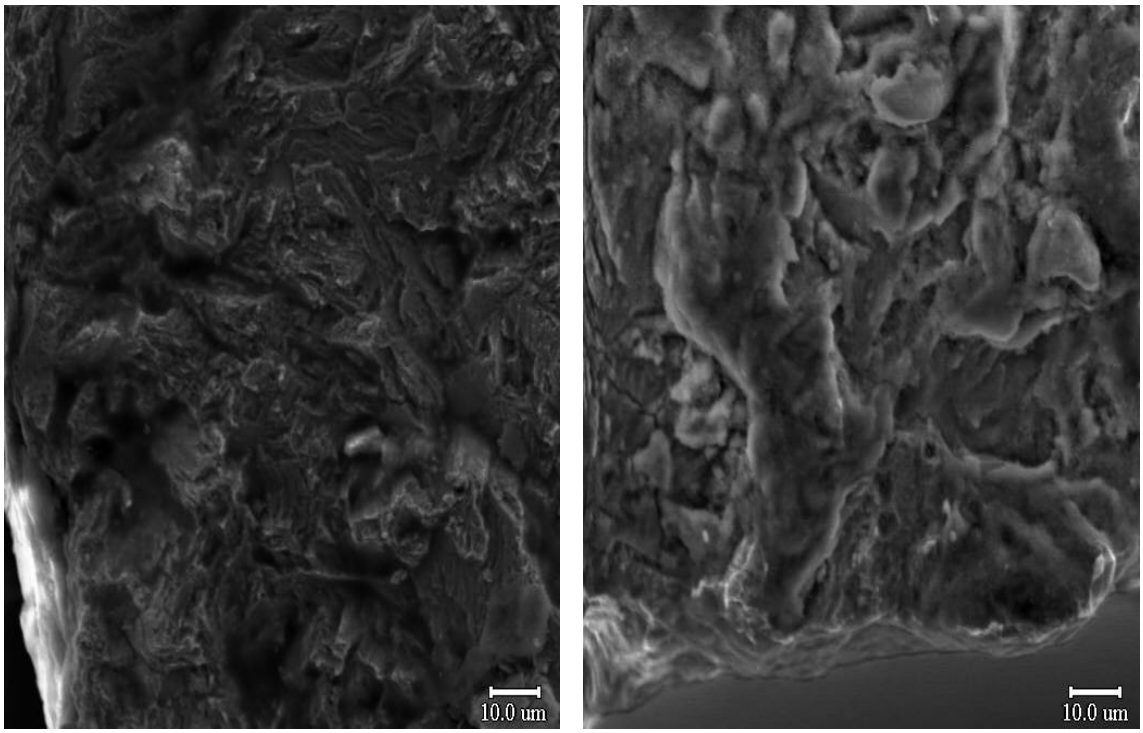

Figure 5.9. Fracture surfaces from batch E
Left: Specimen E1-3 fracture surface (air environment),
Right: Specimen E2-2 fracture surface (aqueous salt environment)

Specimens F1-3 and F2-2 represented batch F. These specimens were both fatigued at a maximum stress of 1000 MPa (145 ksi) and R-value of 0.1. Specimen F1-3

was fatigued in the air environment and experienced 184,398 cycles to failure while the corrosion-fatigued specimen, F2-2, experienced 19,365 cycles to failure. Pictures of both fracture surfaces are found in Figure 5.10.

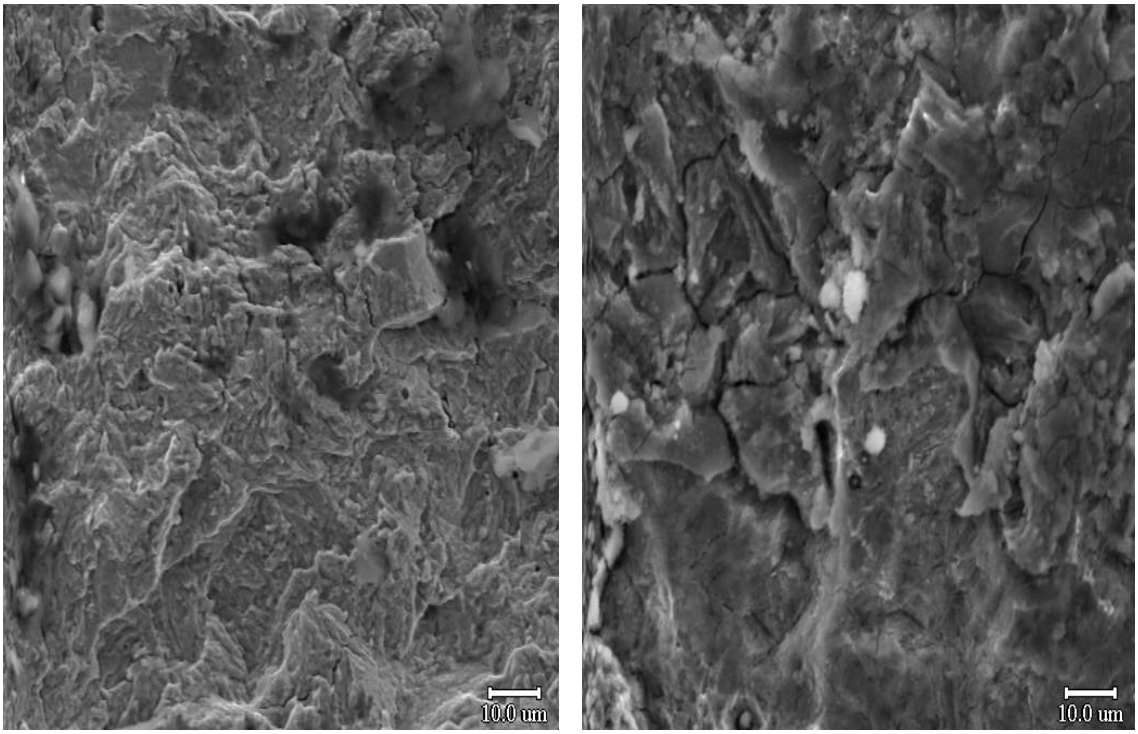

Figure 5.10. Fracture surfaces from batch F
Left: Specimen F1-3 fracture surface (air environment),
Right: Specimen F2-2 fracture surface (aqueous salt environment)

5.6 Discussion

The general trends in the results presented in the previous sections will now be discussed with special consideration to how the data fits into the objectives of this project. Hardness and tensile test results will be discussed, and the relationship between temperature of heat treatment and ultimate tensile strength will be investigated. The trends in the fatigue data from the salt solution and laboratory air are also investigated. Next, the fatigue data is compared to determine the amount of the decrease in fatigue life

that is associated with the corrosive media. Finally, the microstructure and fracture surface is examined to provide insight into the cause of the behavior.

5.6.1 Discussion of Hardness and Tensile Test Results

Based on the results of hardness and tensile testing, the six heat treatment batches fell into one of three groups according to similarities in material properties. Batches A, B, and C were placed in the same group because the low variation in hardness and tensile strength values between them. The maximum difference was 15% for hardness and 14% for tensile strength. This group was known as the lower strength level. Batches D and E were separated by less than 1% in hardness and only 6.5% in tensile strength and were therefore combined to form the middle strength level. The high strength level contained batch F. The difference in strength between the low and medium strength levels was 23%. The difference between the medium and high strength levels was 35%. Therefore, the batches were shown to have some similarities while still representing a wide range of hardness and tensile strength.

The expected trends are noticed in the data shown in Figure 5.1 and Table 5.2. The hardness, yield strength, and tensile strength values increase as the reduction in area and the percent elongation decrease. The trend is caused by increased martensite content giving the steel more strength but less ductility at lower tempering temperatures.

As discussed in previous sections, tempering temperature can be directly related to the microstructure and mechanical properties of steel. For example, a simple plot can demonstrate the linear relationship between ultimate tensile strength and tempering temperature. This relationship is demonstrated in Figure 5.11. The equation for the trend line and the R-squared value is displayed in the graph. The high R-squared value

demonstrates that the trend line closely imitates the data and has a high probability of correctly capturing the behavior. Such a plot can be useful in determining tempering temperatures for a target strength level that optimizes strength and corrosion-fatigue properties.

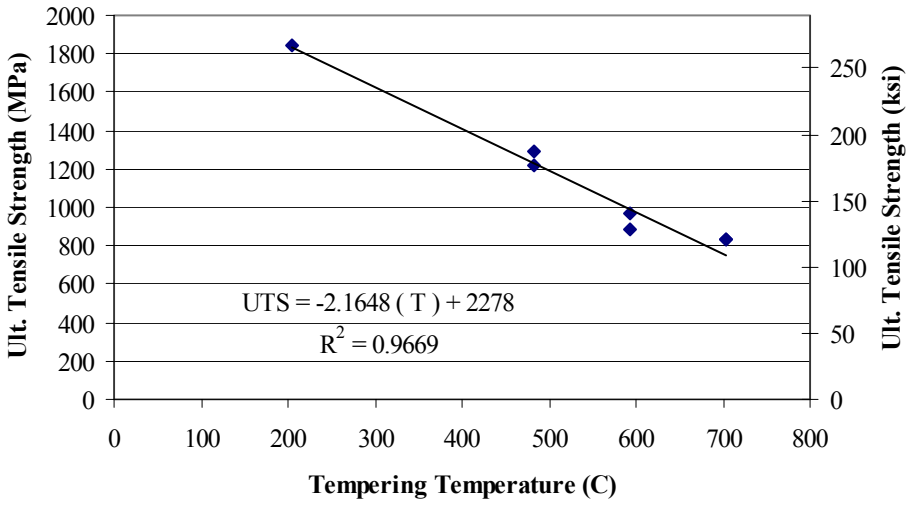

Figure 5.11. Relationship of tempering temperature to ultimate tensile strength

5.6.2 Fatigue Properties in Air Environment

An important trend was apparent in the fatigue results from tests conducted in the laboratory air environment. The well-known relationship of tensile strength to fatigue strength was observed in the data. As was discussed in the background section and demonstrated in Figure 2.6, the relation between fatigue limit and ultimate tensile strength of steel is linear in nature and has a positive slope. Dowling[22] suggests the fatigue limit is approximately half the ultimate tensile strength in most steels. This study demonstrates these trends. The higher strength levels showed longer fatigue lives than the lower strength levels. The trend can be readily observed in Figure 5.12.

Evidence of a fatigue limit was noted in the results. Batches A and D experienced run-outs when the maximum applied stress applied was below 80% of the respective ultimate tensile strength. This behavior is consistent with the concept of a fatigue or endurance limit. It is important to state that fatigue limits are not established by this data, and further testing is needed to establish the precise value of stress below which fatigue failures will not be encountered in this material.

Large variations in fatigue life were observed among the results in the air environment in specimens from various batches. Specifically, the stress versus cycles to failure differs considerably between groups of batches that included batches A, B, and C and those between D, E, and F. Recall that the strength levels of batches A, B, and C were comparable and consistently lower than those grouped as D and E. It is well known that fatigue properties for cycles greater than 10,000 cycles are strongly correlated to the ultimate tensile strength, which is consistent with our observation. On the other hand, the heat treatment F did not exhibit higher fatigue properties compared to conditions D and E. The fatigue properties of extremely high strength and brittle steels such as those in condition F may be influenced by surface flaws that might form during machining of specimens and reduce the fatigue life. The variation in flaw size can also cause large specimen-to-specimen variations among measured fatigue lives under identical conditions.

5.6.3 Fatigue Properties in an Aqueous Salt Environment

In general, the fatigue results conducted in corrosive environment were found to have an opposite trend to that found in the air environment. Lower strength specimens were observed to exhibit longer fatigue lives than higher strength specimens. The trend

is apparent in Figure 5.12 where the normalized maximum stress is graphed versus cycles to failure. For the most part, the corrosion-fatigue data was grouped together in a linear fashion except for the data from batch F. This batch was the highest strength level tested, and it was observed to exhibit the lowest corrosion-fatigue life of all other batches. This clearly demonstrates the severe degradation in fatigue properties due to environment at very high strength levels underscoring the reasons for this study. Thus, the engineer using AISI 4130 steel in corrosive media must consider environmental degradation as a potential failure mechanism. It is well known that fracture toughness of steels such as AISI 4130 decreases with increase in strength, and this study clearly demonstrates that at the higher strength levels, corrosion-fatigue resistance also decreases.

In addition to the trend noted above, the evidence for a fatigue limit that was observed in the air fatigue results was absent in the corrosion-fatigue results. As stated previously, none of the corrosion-fatigue specimens experienced more than 150,000 cycles before failure. This observation shows that the corrosive environment depletes the fatigue limit of low-alloy steel below the stresses that were tested. Because the loading applied in this study was within the normal stress range for this particular steel in service, it was shown that the corrosive environment causes this low-alloy steel to be unacceptable for most structural purposes where the steel is in contact with salt containing media.

The variation in the fatigue results from tests conducted in the corrosive environment was relatively low in comparison to air environment results. As seen in Figure 5.4, the corrosion-fatigue results are tightly grouped while the air environment results show more variation. Results from batch B will be used to illustrate this

observation. When this batch was tested at a stress amplitude of around 530 MPa (76 ksi), there was a difference of 3% in fatigue life between two tests conducted in corrosive environment, but the tests conducted in laboratory air displayed a 166% difference in fatigue life. Similar observations are found in the results for nearly all strength levels.

There could be several reasons for lower variation in the corrosion-fatigue results. As discussed in the background section, several corrosion-fatigue mechanisms are possible that serve to decrease the life that is spent initiating a crack. The three candidate mechanisms that are valid in this material are stress concentrations from pitting, preferential dissolution mechanisms, or the Rebinder mechanism. Each of these mechanisms serves to decrease the variation in corrosion-fatigue data by predictably initiating cracks. Therefore, the variation in flaw size that causes variation in fatigue data generated in laboratory air does not cause the same type of variation in corrosion-fatigue.

Several trends were noticed in the fatigue lives of the various strength levels. First, the crack initiation rate was similar for each strength level. This observation is consistent with the work of Novak, where it was found that crack initiation behavior in a salt solution environment is not particularly dependent on strength or microstructure. Second, the crack propagation rate was determined to be faster for higher strength levels. The conclusion was found since the crack initiation behavior is consistent for all strength levels, yet the total life of the higher strength levels was lower. Therefore, the crack propagation must be faster. Finally, multiple cracks were observed to initiate in the lower strength levels as one proceeded to cause failure. This observation resulted from the increased propagation time associated with the low strength levels that gave more time for subsequent cracks to initiate.

In order to collapse the fatigue data from the air environment into a single trend line to allow comparison with corrosion-fatigue data, the fatigue test results from both environments were normalized by the ultimate tensile strength of each respective batch. Ultimate tensile strength was chosen to normalize the data because it is known to be a contributing factor in determining fatigue strength. As mentioned earlier, Dowling[22] suggests that for most smooth steel specimens, the endurance limit is related to the ultimate tensile strength by a factor of one half. The specimens were tested at maximum stresses ranging from 54% to 93% of their respective ultimate tensile strengths. The trend line for air fatigue data and the normalized fatigue data is illustrated in Figure 5.12 where the hollow symbols designate corrosion-fatigue results and the solid symbols denote fatigue results from the air environment.

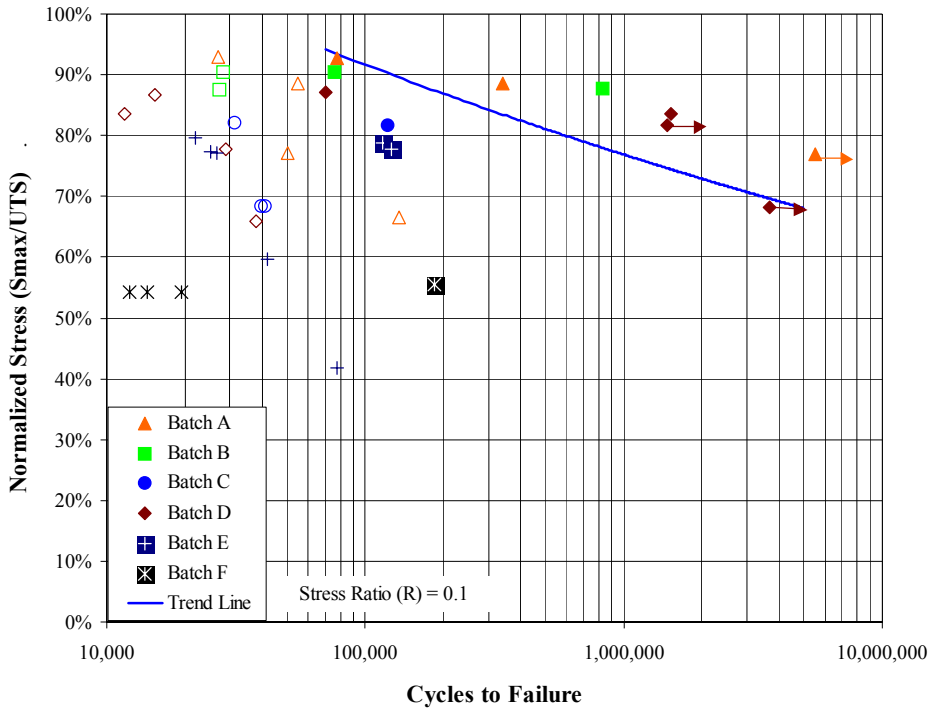

Figure 5.12. Normalized combined fatigue data for various strength levels. The solid symbols indicate tests in air and the hollow symbols indicate tests in corrosive environment.

By normalizing the fatigue data, a comparison can be made between the fatigue life in corrosive media and in air of the various heat treatments. The result of this comparison is shown in Figure 5.13 organized by batch letter. The error bars shown in the figure represent one standard deviation above and below the average fatigue life. The standard deviation in the fatigue data obtained from the air environment is in some cases quite large. A possible reason for this observation was discussed previously.

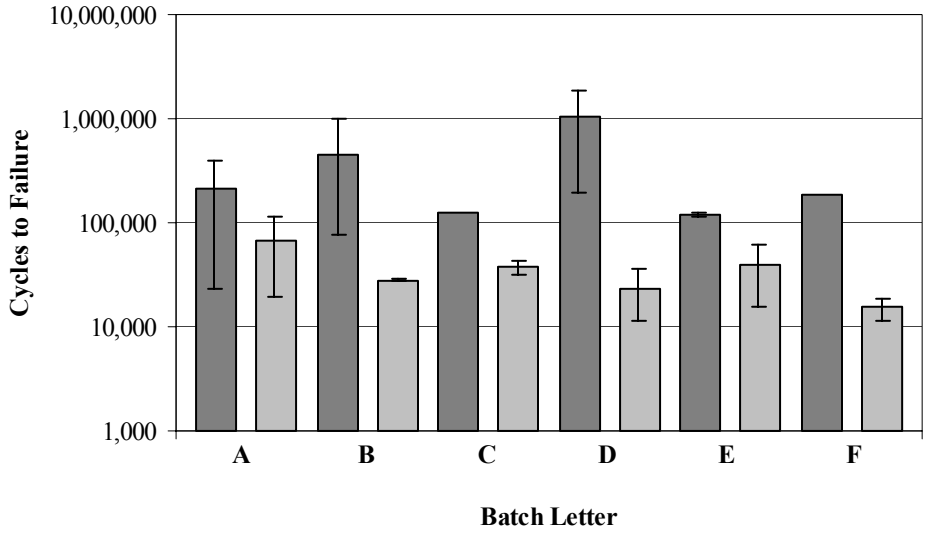

Figure 5.13. Comparison of fatigue lives obtained in air and in corrosive media. The darker color bars refer to tests in air and the lighter color bars are for tests in corrosive environment.

The difference in the average fatigue life between the air and corrosive environments was calculated for each batch. This difference was divided by the average fatigue life in air to obtain the percent drop in fatigue life for each batch. The result of this calculation is illustrated in Figure 5.14.

As is noticed in Figure 5.14, the results seem to fall in two groups. One group shown in light gray includes batches A, B, and D and the other group shown in dark gray

includes C, E, and F. The differences between the two groups are that batches A, B, and D were heat treated at Bodycote Thermal Processing, and batches C, E, and F were heat treated by Braddock Metallurgical. The two groups were also taken from different batches of material and tested during different time periods. The combination of these differences is believed to be the reason for the discrepancy in the data.

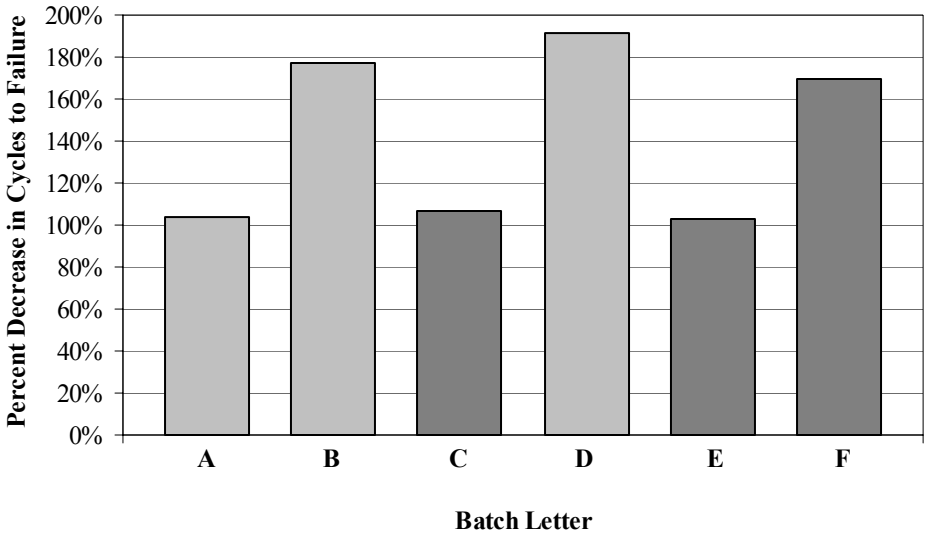

Figure 5.14. Percent difference in the fatigue life between air and salt water (light color represents HT by Bodycote, dark color represents HT by Braddock)

Within the two groups, the data demonstrates a trend that is consistent with the findings of many corrosion scientists. This trend was discussed in the background section and illustrated in Figure 2.6. Both groups show that higher strength levels result in larger detriment to the fatigue life caused by the corrosive media. Batches A, B, and D display decreases in fatigue life ranging from 103% for batch A to 191% for batch D. Batches C, E, and F, on the other hand, show decreases ranging from 106% for batch C to 170% for batch F. Although the scale of the detriment seems to be different between the groups, the expected trend is evident in this data.

An additional observation from Figure 5.14 is that there is a grater amount of variation between the results from batches C, E, and F. These three batches were processed at Braddock Metallurgical in Atlanta, Georgia. The differences in processing and testing that caused the variation were not identified in this study although they would be useful for understanding the effect that processing has on fatigue life. This issue is discussed further in the Recommendations section.

The optimum condition that combines strength, fracture toughness, and corrosion-fatigue resistance in this steel might well be a heat treatment that results in medium strength levels such as condition C in this study. This strength level is approximately 964 MPa (140 ksi). From Figures 5.12 and 5.13, it is noted that this strength level exhibits the smallest decrease in fatigue resistance in the salt-water environment under the imposed conditions and the corrosion-fatigue resistance is high. These figures also show that corrosion-fatigue might well be the limiting mechanical property in the application of AISI 4130 steels in corrosive environments. However, the amount of data available to support this conclusion is limited, and it is recommended that additional testing be pursued to further strengthen the basis for such a conclusion.

5.6.5 Relationship of Microstructure and Fracture Surface to Test Results

As was shown in Section 5.5.1 on microstructure, the higher strength specimens of this study display a higher percentage of martensite than the lower strength specimens. Increased martensite content can also be linked to high hardness, tensile strength, and fatigue strength in low-alloy steel. As an example, batch F demonstrated the highest hardness and strength and also displayed a typical martensitic microstructure.

As shown in the results of this study, an increase in strength level signifies an increase in the susceptibility to corrosion-fatigue. Since martensite is known to be the strengthening phase in this steel, it is suspected to be the cause of this effect. It should be noted that the same phase that produces the desirable increases in hardness, strength, and fatigue resistance in benign environments, is also the phase that contributes to undesirable corrosion-fatigue performance.

The apparent grain size of the various heat treatments used in this project were observed to be of similar size in the various pictures of the microstructure found in Section 5.5.1. Therefore, it appears that this steel does not follow the conventional Hall-Petch relationship that says that a material is strengthened by reducing grain size. Since the grain size does not significantly change between the strength levels, there must be another strengthening mechanism involved in this material. The strengthening mechanism observed in this steel is the phase change associated with quenching and tempering. In this case, martensite and fine bainite are the microstructural parameters that contribute to the strength of this steel.

In Section 5.5.2, the fracture surfaces of specimens fatigued at similar maximum stresses were compared. There are two observations to be made from this comparison. The first is that each of the three batches (C, E, and F) showed similar cracking behavior in the air environment. The general appearance of the fracture surfaces showed that the mode of cracking was mainly transgranular with some cleavage type facets as was observed in a study by Tau on the same material.[8] The second observation was that the mode of cracking is similar in both environments. On the fracture surface of the corrosion-fatigue specimens, the surface features appeared more rounded, and it was

concluded that a typical oxide layer covered the material's surface. This layer, which is a typical byproduct of the corrosion process, essentially destroys the underlying material microstructure. Instead of removing the oxide layer, the relative similarities between the fracture surfaces were used to conclude that both environments resulted in transgranular type cracks. This conclusion was sufficient for the purposes of this research. The fact that transgranular cracking was observed in each strength level for both environments showed that the crack propagation was not particularly dependent on mechanical properties.

The data reported earlier that shows decreased fatigue life of this steel when exposed to the corrosive environment and the findings in the previous paragraph demonstrate that the corrosive environment enhanced the crack growth while not changing the mode of cracking. Therefore, the decrease in fatigue life was associated with initiation rather than propagation of the crack.

CHAPTER VI

CONCLUSIONS

This study investigated the decrease in fatigue life associated with immersion of AISI 4130 steel heat treated to strengths ranging from 896 MPa to 1862 MPa (121 – 268 ksi) in an aqueous sodium chloride based environment. The environment consisted of 0.5% NaCl, 0.1% $CaCl_2$, and 0.075% $NaHCO_3$ dissolved on a weigh percent basis in DI water and was designed to simulate an aggressive field environment. The fatigue loading included a continuous constant-amplitude cyclic loading with a stress ratio of R = 0.1 that was applied at a frequency of 1 Hz. The following observations were found in response to the objectives of this research:

1. Decreases in fatigue life caused by the corrosive environment ranged from 100% in the lowest strength level to 190% in the higher strength levels. This result showed that higher strength in this steel corresponds to increasing detriment to fatigue life when exposed to an aqueous salt environment.
2. The optimum condition of this steel that combined strength, fracture toughness, and corrosion-fatigue resistance is believed to be condition C. This heat treatment batch had a strength level around 964 MPa (140 ksi) and it exhibited high corrosion-fatigue resistance when compared to the other strength levels.
3. The fact that signs of a fatigue limit were evident in the air environment but absent in the salt solution led to the conclusion found by other researchers[6]

that there is no “safe stress range” that provides satisfactory corrosion-fatigue performance in this steel.

4. The decrease in fatigue life between environments was attributed to the presence of martensite in the structure of the steel. It was noted that the higher the martensite content, the larger the decrease in fatigue life when exposed to the corrosive environment.
5. The fracture surfaces of fatigued specimens revealed that a similar cracking mode was present for each strength level in both environments. Enhanced crack initiation was, therefore, assumed to be the cause of the decrease in fatigue life between the air and aqueous salt environments.

The above observations satisfactorily characterized the corrosion-fatigue behavior of this steel and provide useful information that may be used in design situations that require high strength low-alloy steel in environments such as the one studied here.

CHAPTER VII

RECOMMENDATIONS

The goal of this project was to determine the decrease in fatigue life that is associated with AISI 4130 steel in an aqueous salt environment. To add to the significance of the documented results, several recommendations for future work are discussed in the following paragraphs. There are three main areas in which this research could be expanded to provide more meaningful results for the designer using low alloy steel in a corrosive environment. These three include having more data, investigating other variables, and exploring the source of variation in the data.

The first item that would improve the scope of this study would be the ability to obtain more fatigue results. With more data, statistical techniques could be employed to give insight into the true nature of the behavior of this material. As it was, the statistical scatter was too large, and the data set too small to obtain accurate calculations other than average and standard deviation. Another beneficial result of more data includes the ability to determine the fatigue limit associated with the air environment for each strength level. The fatigue limit in air would provide a starting point to which the corrosion-fatigue data could be compared. One other benefit of further testing would be the ability to fatigue test at lower stress amplitudes in the corrosive environment to explore fatigue limit behavior. An estimation of the fatigue limit in corrosive environment would be beneficial from a design point of view. If the fatigue limit for this steel in both environments was found, it could offer a more meaningful comparison between the

behaviors of various strength levels than the differences in fatigue life that were compared in this study.

The second item that would serve to expand the results of the study is the investigation of other variables that affect the corrosion-fatigue properties of this steel. Load ratio, load frequency, and temperature are known to affect corrosion-fatigue behavior of metals. Varying each variable in a carefully designed experiment would allow designers to have a more comprehensive knowledge of the true corrosion-fatigue behavior of this steel. The pH of the salt solution used in this study is also expected to affect corrosion-fatigue behavior. An interesting investigation could include varying the pH and determining effects associated with pH level.

The third point that could be investigated is the variation in the fatigue results from batches C, E, and F. It was observed in the results of fatigue testing that these three batches displayed more variation than the other three. Batches C, E, and F were thermally processed in a different location than the other three batches. They were also tested during a different time period than the other batches. The specific cause of the variation would be interesting to determine so that manufacturers could be sensitive to the processing variations that cause fatigue life variation.

APPENDIX

DATA AND CALCULATIONS

Table A.1. Rockwell C Hardness Data

Batch A		Batch B		Batch C		Batch D		Batch E		Batch F	
A-1	23.1	B-1	25.9	C1-1	26.5	D-1	37.3	E1-1	37.4	F1-1	47.1
A-2	23.2	B-2	25.2	C1-2	26.5	D-2	37.5	E1-2	37.6	F1-2	45.8
A-3	22.2	B-3	24.9	C1-3	26.5	D-3	38.0	E1-3	37.6	F1-3	47.4
A-4	23.1	B-4	25.6	C2-1	27.0	D-4	37.6	E1-4	37.1	F2-1	45.8
A-5	22.9	B-5	25.6	C2-2	29.2	D-5	37.2	E1-5	36.7	F2-2	49.8
A-6	23.4	B-6	25.8	C2-3	26.7	D-6	37.3	E2-1	38.5	F2-3	48.5
A-7	23.2			C2-4	26.1	D-7	37.1	E2-2	38.8	F2-4	
A-8	22.2			C2-5	30.3	D-8	37.3	E2-3	35.3	F2-5	51.3
A-9	23.5			C2-6	23.3	D-9	37.5	E2-4	38.3	F2-6	
A-10	23.3					D-10	38.1	E2-5	39.8		
								E2-6	38.6		
Average =	23.0	Average =	25.5	Average =	26.9	Average =	37.5	Average =	37.8	Average =	48.0
Std. Dev. =	0.46	Std. Dev. =	0.38	Std. Dev. =	1.97	Std. Dev. =	0.33	Std. Dev. =	1.21	Std. Dev. =	2.05

Table A.2. Dimensions of Specimens and Tensile Test Data

Specimen Designation	Dimensions		Tensile Test Data			
	Width (in.)	Thickness (in.)	% Elongation	% Red. in Area	0.2% Yield (psi)	UTS (psi)
A-1	0.251	0.230	25.6%	60.8%	106,882	121,455
A-2	0.251	0.230	24.7%	60.0%	106,588	121,358
B-1	0.251	0.230	23.8%	61.1%	117,877	128,815
C1-2	0.250	0.241	18.6%	60.9%	125,500	138,700
C1-3	0.250	0.241	18.7%	60.9%	113,300	140,800
D-1	0.251	0.230	10.6%	56.0%	169,274	175,377
D-2	0.251	0.230	16.8%	54.8%	169,206	176,962
E1-1	0.250	0.241	13.3%	49.8%	180,000	188,800
E1-2	0.250	0.241	13.6%	50.9%	176,400	187,100
F1-1	0.251	0.241	12.4%	44.2%	194,000	269,400
F1-2	0.250	0.242	12.3%	44.7%	185,000	266,200

Table A.3. Fatigue Test Data from Air and Corrosive Environment

		Dimensions			Fatigue Data												Max Stress /	
Heat Treat	Spec. (#)	Width (in.)	Thick. (in.)	Test Type	Freq. (Hz)	Loading (max lbf)	Loading (min lbf)	Stress max/min (max ksi)	Stress max/min (min ksi)	Stress max/min (max MPa)	Stress amp/mean (Sa ksi)	Stress amp/mean (Sm ksi)	Sar (ksi)	Sar (Mpa)	Cycles to Failure	Yield (%)	UTS (%)
A-3	R/O	0.251	0.230	air	10	5400	540	93.5	9.3	644.4	42.1	51.4	62.7	432.3	5,500,000	88%	77%
R/O	2,255,200	0.251	0.230	air	10	5800	580	100.4	10.0	692.1	45.2	55.2	67.3	464.3		94%	83%
A-4		0.251	0.230	air	10	6200	620	107.5	10.8	741.4	48.4	59.1	72.1	497.3	341,347	101%	89%
A-5		0.251	0.230	air	10	6500	650	112.6	11.3	776.6	50.7	62.0	75.6	521.0	77,843	106%	93%
A-6		0.251	0.230	salt	1	5400	540	93.6	9.4	645.4	42.1	51.5	62.8	433.0	49,921	88%	77%
A-7		0.251	0.230	salt	1	6200	620	107.4	10.7	740.8	48.3	59.1	72.1	496.9	54,918	101%	88%
A-8		0.251	0.230	salt	1	6500	650	112.7	11.3	777.2	50.7	62.0	75.6	521.4	27,102	106%	93%
A-9		0.251	0.230	salt	1	4650	465	80.8	8.1	557.0	36.4	44.4	54.2	373.6	134,976	76%	67%
B-2		0.250	0.230	air	10	6500	650	113.1	11.3	779.7	50.9	62.2	75.9	523.1	828,156	96%	88%
B-3		0.250	0.230	air	10	6700	670	116.4	11.6	802.5	52.4	64.0	78.1	538.3	75,955	99%	90%
B-4		0.251	0.230	salt	1	6500	650	112.8	11.3	777.6	50.8	62.0	75.7	521.6	27,413	96%	88%
B-5		0.250	0.230	salt	1	6700	670	116.5	11.6	803.1	52.4	64.1	78.1	538.7	28,324	99%	90%
C2-5	2 5	0.252	0.240	air	20	6920	692	114.3	11.4	787.9	51.4	62.9	76.7	528.6	122,064	96%	82%
C2-3	2 3	0.251	0.241	salt	1	5800	580	95.7	9.6	660.0	43.1	52.6	64.2	442.7	40,998	80%	68%
C2-4	2 4	0.252	0.241	salt	1	5800	580	95.5	9.6	658.5	43.0	52.5	64.1	441.7	39,719	80%	68%
C2-6	2 6	0.251	0.240	salt	1	6920	692	114.7	11.5	791.1	51.6	63.1	77.0	530.7	31,223	96%	82%
D-3		0.251	0.230	air	10	8500	850	147.3	14.7	1015.6	66.3	81.0	98.8	681.3	1,529,085	87%	84%
D-4	R/O	0.250	0.230	air	10	6920	692	120.2	12.0	828.4	54.1	66.1	80.6	555.7	3,665,881	71%	68%
R/O	2,154,823	0.250	0.230	air	10	7900	790	137.2	13.7	945.8	61.7	75.4	92.0	634.4		81%	78%
D-5		0.250	0.229	air	10	8800	880	153.5	15.3	1058.1	69.1	84.4	102.9	709.8	70,105	91%	87%
D-10	R/O	0.251	0.230	air	10	8300	900	143.9	15.6	992.1	64.1	79.7	96.5	665.5	1,476,360	85%	82%
D-6		0.251	0.230	salt	1	6700	670	116.2	11.6	800.8	52.3	63.9	77.9	537.2	38,013	69%	66%
D-7		0.251	0.230	salt	1	8500	850	147.4	14.7	1016.0	66.3	81.0	98.8	681.5	11,647	87%	84%
D-8		0.250	0.230	salt	1	8800	880	152.9	15.3	1053.9	68.8	84.1	102.5	707.0	15,327	90%	87%
D-9		0.251	0.230	salt	1	7900	790	137.0	13.7	944.3	61.6	75.3	91.9	633.4	28,945	81%	78%
E1-3	1 3	0.250	0.241	air	1	8934	1121	148.3	18.6	1022.4	64.8	83.4	99.5	685.8	117,165	83%	79%
E2-5	2 5	0.252	0.245	air	10	9000	900	146.0	14.6	1006.3	65.7	80.3	97.9	675.1	125,559	82%	78%
E1-4	1 4	0.250	0.239	salt	1	8944	1020	149.7	17.1	1032.1	66.3	83.4	100.4	692.3	21,979	84%	80%
E1-5	1 5	0.250	0.239	salt	1	4700	470	78.7	7.9	542.3	35.4	43.3	52.8	363.8	77,876	44%	42%
E2-6	2 6	0.252	0.245	salt	1	6920	692	112.2	11.2	773.4	50.5	61.7	75.2	518.8	41,914	63%	60%
E2-1	2 1	0.252	0.244	salt	1	8935	1002	145.2	16.3	1001.4	64.5	80.8	97.4	671.8	25,264	82%	77%
E2-2	2 2	0.253	0.245	salt	1	8948	1005	144.9	16.3	998.9	64.3	80.6	97.2	670.1	26,781	81%	77%
F1-3	1 3	0.251	0.240	air	1	8941	1028	148.4	17.1	1023.3	65.7	82.7	99.6	686.5	184,398	78%	55%
F2-1	2 1	0.252	0.245	salt	1	8950	1018	145.3	16.5	1001.5	64.4	80.9	97.4	671.8	14,270	77%	54%
F2-2	2 2	0.252	0.244	salt	1	8946	1003	145.2	16.3	1001.1	64.5	80.7	97.4	671.6	19,365	77%	54%
F2-3	2 3	0.252	0.245	salt	1	8946	1004	145.2	16.3	1001.1	64.4	80.7	97.4	671.5	12,180	77%	54%

Table A.4. Fatigue Data Comparison (run-outs were not used in calculations)

Batch	A	B	C	D	E	F
Fatigue Life in Air Environment	209,595	452,056	122,064	1,025,183	121,362	184,398
Fatigue Life in Aq. Salt Media	66,729	27,869	37,313	23,483	38,763	15,272
Difference	142,866	424,187	84,751	1,001,700	82,599	169,126
%Decrease	103%	177%	106%	191%	103%	169%

Batch	A	B	C	D	E	F
Std. Deviation in Air Environment	186,325	531,886	0	827,542	5,935	0
Std. Deviation in Aq. Salt Media	47,081	644	5,313	12,214	23,169	3,696

REFERENCES

1. Pourbaix, M. (1966). *Atlas of electrochemical equilibria in aqueous solutions.* New York: Pergamon Press, pp. 307-321.

2. Scott, P. M. (1983). Chemistry effects in corrosion-fatigue. *Corrosion-fatigue: Mechanics, metallurgy, electrochemistry, and engineering, ASTM STP 801*. T. W. Crooker, & B. N. Leis (Eds.). West Conshohocken: American Society for Testing and Materials, pp. 319-350.

3. Suresh, S. (1998). *Fatigue of materials* (2nd Ed.). New York: Cambridge University Press.

4. Novak, S. R. Corrosion-fatigue crack initiation behavior of four structural steels. *Corrosion-fatigue: Mechanics, metallurgy, electrochemistry, and engineering, ASTM STP 801*. T. W. Crooker and B.N. Leis (Eds). West Conshohocken: American Society for Testing and Materials, pp. 26-63.

5. Laird, C., & Duquette, D. J. (1971). Mechanisms of fatigue crack nucleation. *Corrosion-fatigue: Chemistry, mechanics, and microstructure.* Houston: National Association of Corrosion Engineers, pp. 88-115.

6. Boyer, H. E. (Ed.). (1986). *Atlas of fatigue curves*. Metals Park: American Society for Metals, pp. 1-12.

7. Zhu, Z. Y., Farrington, G. C. and Land, C. (1987). Fatigue crack initiation and propagation in AISI 4130 steel exposed to neutral perchlorate solution. *Materials Science and Engineering,* 91, pp. 125-135.

8. Tau, L., Chan, S. L. I. & Shih, C. S. Hydrogen enhanced fatigue crack propagation of bainitic and tempered martensitic steels. *Corrosion science,* 38(11) pp. 2049-2060.

9. Kitagawa, H. (1971). A fracture mechanics approach to ordinary corrosion-fatigue of unnotched steel specimens. *Corrosion-fatigue: Chemistry, mechanics, and microstructure*. Houston: National Association of Corrosion Engineers, pp. 521-528.

10. McEvily, A. J., Jr. (Ed.). (1990). *Atlas of stress-corrosion and corrosion-fatigue curves*. Materials Park: ASM International, p. 112.

11. Fujii, C. T. & Smith, J. A. (1983) Environmental influences on the aqueous fatigue crack growth rates of HY-130 steel. *Corrosion-fatigue: Mechanics, metallurgy, electrochemistry, and engineering*, *ASTM STP 801*.T. W. Crooker & B. N. Leis

(Eds.). West Conshohocken: American Society for Testing and Materials, pp. 390-402.

12. Van der Velden, R., Ewalds, H. L., Schultze, W. A., & Punter, A. (1983). Anomalous fatigue crack growth retardation in steels for offshore applications. *Corrosion-fatigue: Mechanics, metallurgy, electrochemistry, and engineering*, *ASTM STP 801*. T. W. Crooker & B. N. Leis (Eds.) West Conshohocken: American Society for Testing and Materials, pp. 64 – 80.

13. Le May, I., & Beltran, N. O. (1986). Metallography and fractography in corrosion-related failures. *Metallography and corrosion*. Houston: National Association of Corrosion Engineers, pp. 119-130.

14. Bamford, W. H. (1983). Implementing corrosion-fatigue crack growth rate data for engineering applications. *Corrosion-fatigue: Mechanics, metallurgy, electrochemistry, and engineering, ASTM STP 801*. T. W. Crooker & B. N. Leis (Eds.). West Conshohocken: American Society for Testing and Materials, pp. 405-422.

15. Philip, T. V. (1999) Ultrahigh-strength steels. *ASM handbook,* Volume 1, *Properties and selection: Irons, steels, and high performance alloys,* ASM International, in *ASM Handbook on CD-ROM,* ASM International and The Dialog Corporation. Retrieved December 2, 2003.

16. Rice, R. C., Jackson, J. L., Bakuckas, J. & Thompson, S. (2003) Metallic materials properties development and standardization (MMPDS), U.S. Department of Transportation/Federal Aviation Administration Report, pp. 2.10 – 2.38.

17. Thelning, K. E. (1984). *Steel and its heat treatment.* Boston: Butterworths, pp. 6-22.

18. ASTM E 8. (2003). American society for testing and materials publication. West Conshohocken, PA: Author.

19. ASTM E 18. (2003). American society for testing and materials publication. West Conshohocken, PA: Author.

20. ASTM 466. (1966). American society for testing and materials publication. West Conshohocken, PA: Author.

21. Society of Automotive Engineers. (SAE) J2334. (1998). Cosmetic corrosion lab test. Warrendale, PA: Author.

22. Dowling, N. E., *Mechanical behavior of materials,* (2nd ed.). (1999). New York: Prentice Hall International, Inc., pp. 380-390.